university of groningen

Robust Estimation of the Temperature Profile of a Stratified Thermal Storage Tank

Bachelor Integration Project
Industrial Engineering and Management

Author:
R.J. van Driezum
S3788709

First supervisor:
prof. dr. ir. J.M.A. Scherpen
J.A. Machado Martinez

Second supervisor:
prof. dr. ir. M. Taheri

January 29, 2023

Abstract

Global warming has been a crucial topic for the last decades. District Heating can play a significant role in reducing energy usage and CO_2 emissions. This research aims to review different types of observer designs for estimating the temperature profile of a stratified thermal storage tank in district heating applications. First, the mathematical model for a stratified thermal storage tank is deducted from the literature and includes the slow buoyancy and mixing terms, in addition to most mathematical descriptions. Literature research on the Sliding Mode is conducted, and the essential operation of the Sliding Mode is elucidated. For the Sliding Mode Observer Design, a bounded disturbance function is fundamental. This research conducts literature research on all parameters to check their possible disturbance. From all gathered possible disturbance per parameter, a bounded disturbance function is designed which can be utilized. Different Sliding Mode Observer designs are explained, and there is shown that each design with a disturbance does not match a fundamental matching condition needed for the implementation of the observer. The research proves that the mathematical model, as depicted, cannot be observed by a Sliding Mode Observer. This thesis proposes a narrowed-down error function that enables the design of a Sliding Mode Observer. This narrowed-down system does not converge within a reasonable time. However, for fictional values of the parameters, the Sliding Mode Observer partially holds, proving its potential for other mathematical systems.

Contents

List of Figures

List of Tables

Abbreviations

DHS	District Heating System
HVAC	Heating, cooling, ventilation and air conditioning
CHP	Combined Heat and Power Plant
TES	Thermal Energy Storage
SoC	State of Charge
SES	State Estimation Strategies
PDE	Partial Differential Equation
ODE	Ordinary Differential Equation

Nomenclature

α	Fluid Diffusivity $[m^2/s]$
Δz	Thickness of the layer $[m]$
$\dot{m}_i$	Input flow [kg/s]
$\dot{Q}_i$	External input heat [J]
η	Scaling parameter in the approximation of the step function [ ]
$\hat{T}$	Temperature estimation $[^\circ C]$
μ	Scaling factor for the approximation of the max function the slow buoyancy [ ]
ρ	Density [kg/m^3]
A	Cross-sectional area [m]
c_p	Specific heat [J/kg $^\circ C$]
k	Thermal Conductivity of the isolation wall $[W/(m^\circ C)]$
P	Perimeter of the tank $[m]$
$S(T_2 - T_1)$	Step function with a value of either 1 or 0 [ ]
T_i^{in}	Temperature of the input flow $[^\circ C]$
T_∞	Ambient temperature $[^\circ C]$
T_i	Temperature at layer i $[^\circ C]$

Notations and Symbols

$\mathbb{R}$ = all real numbers

$\in$ = belongs to

$\subset$ = subset of

$\forall$ = for all

$\mathbb{R}_+$ = all real positive numbers ($x > 0 \quad \forall \quad x$)

$\mathbb{R}^n$ = a $n \times 1$ vector $\in \mathbb{R}$

$\mathbb{R}^{m \times n}$ = matrix of size $m \times n \in \mathbb{R}$

A^T or x^T = the transpose of matrix A, or vector x

$\rightarrow$ = tends to

$\implies$ = implies

$\sum$ = summation

$\dot{x}$ = derivative of x with respect to time

$|x|$ = absolute value of x

$||x||$ = norm of x

$\frac{\partial x}{\partial t}$ = partial derivative of x with respect tot t

$f : V \rightarrow \mathbb{R}$ = a function mapping V into $\mathbb{R}$

$[a, b]$ = set of all numbers x satisfying $a \leq x \leq b$

(a, b) = set of all numbers x satisfying $a < x < b$

$TD - 1$ = the inverse of matrix D

$col(x1, x2) = \begin{bmatrix} x1 \\ x2 \end{bmatrix}$

$\wedge$ = and

1 Introduction

Global warming is causing extreme weather, such as floods, heat waves, and storms [21] [19]. These extreme weather events have a severe impact on both humans and animals. The energy transition has, therefore, taken up an important role in the world. Heating, cooling, ventilation and air conditioning (HVAC) of buildings takes up approximately 50% of the total energy consumption of Europe [20]. Showing that a more sustainable way of heating and cooling buildings is key in the energy transition.

District heating and cooling can play a vital role in this transition if the technology is implemented and optimized [18]. This is shown by [11], who showed that switching from a typical boiler or heat pump to a District Heating System (DHS) with a Combined Heat and Power Plant (CHP) in combination with house envelope and isolation measures can reduce the primary energy use by 88% and the CO2 emissions by 96%. Figure 1 shows that a DHS consists of a centralized large power plant, the transmission that is transported through pipes, the end users, and the thermal storage [20]. Figure 1 shows that Thermal Storage experiences losses of up to 80%, which badly impacts the overall system's efficiency and sustainability.

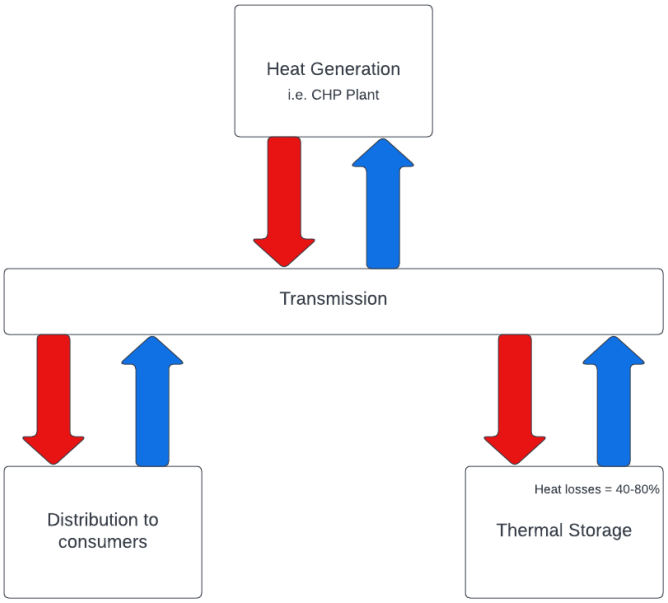

Figure 1: *Simplified illustration of a DHS derived from [20]*

Thermal Energy Storage (TES) in a DHS can be stored in three main ways, namely sensible heat storage, latent heat storage, and chemical heat storage [8]. The aim of this project will be sensible heat storage with a specific focus on stratified thermal storage tanks. Stratification in storage tanks has been shown to improve the performance of the heat storage [23]. Stratification in storage tanks entails that there exists a temperature profile throughout the whole tank. As cold water is denser than hot water, hotter water remains at the top while cold water stays at the bottom. Stratification improves the effectiveness of the heat storage [5]. An essential aspect of these thermal storage tanks is knowing when to tap and when to load hot and cold water. The execution of the loading and tapping can be performed with a controller. The total energy of a thermal storage tank can be determined with the State of Charge (SoC) of a tank. The SoC is the ratio between the current energy in a thermal storage tank, which is compliant with the users' needs, and the maximum amount of energy in a thermal storage tank [32]. Calculating the SoC relies on the temperature at any given point within the tank [22]. Therefore, the temperature profile of a stratified thermal storage tank needs to be mapped.

Sensors can be used for this, but hardware purchases should be minimized to reduce costs, and sensors are prone to both failure and malfunctioning. State Estimation Strategies (SES) can be used to estimate the temperature profile of a stratified thermal heat tank as shown in [16], who shows the comparison between different SES. This research did not account for possible noise or parameter uncertainty in the system, which has to be taken into account, as noise [35] or parameter uncertainty can alter the measured temperature. For such systems, a more robust estimation of the temperature profile needs to be observed with a SES that also complies to a low error margin. A couple of essential aspects for such an observer are that the observer should not have a long calculating time, which will counter the need for such an observer. The observer should also not be resource intensive; otherwise, a lot of sensors could be used as well. The server should also be compatible with control strategies that apply to controlling thermal storage tanks.

2 System Description

2.1 System Model

The system in this project will be much smaller than an overall DHS. The system will consist only of the thermal storage tank, as shown in Figure 2. Figure 2 shows a DHS with a CHP as a heat producer. The stratified thermal storage tank, as shown in the middle, will be the complete system in this research. As the inflow and outflow of the tank do have a serious impact on the content of the tank, they are also considered part of the system. In this report, the modeling will be performed on a tank with five layers. However, the mathematical model will be explained with n layers. As this research will focus on estimating the temperature profile of the whole stratified thermal storage tank, the only temperature sensors present will be at i=1 and i=n, hereby simulating how the SES could work in real-time applications.

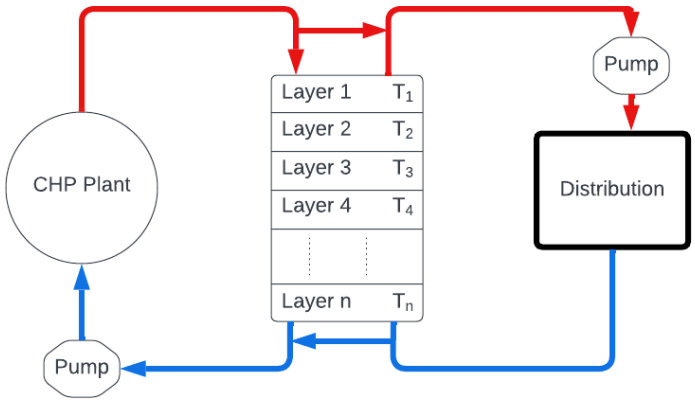

Figure 2: *District Heating and Cooling System derived from [22]*

2.2 Mathematical Model

2.2.1 Working Assumptions

This research makes multiple working assumptions so the system can be used for optimization strategies. The following six working assumptions are made in order to keep the system simple:

1. The system will be simplified into a 1-dimensional model by discretizing the mathematical model. This simplification shall ensure that the system is less computationally heavy, which makes it both easier and faster to estimate the temperature. At the same time, it is proven that a 1-dimensional model gives very reliable results for stratified thermal storage tanks [24].
2. It is assumed that all the layers have the same height, perimeter, cross-sectional area, and thermal conductivity of the isolation wall.
3. It is assumed that the variable of interest for each control volume (layer i) will be the average temperature throughout the whole layer.
4. During the design and modeling of the observer, a tank with three layers will be used as three layers describe the system's complete physics whilst not complicating the research.
5. It is assumed that while loading the tank in either layer 1 or 3, it will unload at the same time from the other layer, keeping the volume in the tank constant. In this case, (un)loading means water entering or leaving the tank.
6. It is assumed that the charging only happens through loading in layer one discharging only happens through loading in layer 3

2.2.2 Mathematical Description

Besides the visualized system in 2, the temperature of each layer in the thermal storage tank can also be described mathematically with a Partial Differential Equation (PDE) [17]. In a real stratified thermal storage tank, the temperature difference is not divided into layers but differs gradually in the tank. However, this system is too complex for optimization purposes. Therefore, as discussed in the working principles, the tank will be discretized in layers where the temperature is uniform throughout the whole layer.

The following PDE [17] describes the state of a layer i:

$$\frac{\partial T_i}{\partial t} = \underbrace{\alpha \frac{\partial^2 T_i}{\partial z^2}}_{\text{heat flux}} + \underbrace{\frac{P_i k_i}{\rho c_p A_i}(T_\infty - T_i)}_{\text{heat loss environment}} + \underbrace{\frac{\dot{Q}_i}{\rho c_p A_i z_i}}_{\text{Indirect (dis)charging}} + \underbrace{\frac{\dot{m}_i(T_i^{in}) - T_i}{\rho A_i z_i}}_{\text{Direct dis(charging)}} + \underbrace{\lambda}_{\text{Slow Buoyancy}} + \underbrace{\phi}_{\text{Mixing}} \tag{2.1}$$

Equation 2.1 still has a second order derivative. This second order derivative has to be discretized in space to simplify the system, transforming the PDE into an Ordinary Differential Equation (ODE). PDE (2.1) can be discretized using the finite difference method [31], together with applying working assumption 2 will result in 2.2.

$$\frac{dT_i(t)}{dt} = \alpha \frac{T_{i+1} - 2T_i + T_{i-1}}{z^2} + \frac{K}{\rho c_p A}(T_\infty - T_i) + \frac{\dot{Q_{k,i}}}{z \rho c_p A} + \frac{\dot{m}_i}{z \rho A}(T_i^{in} - T_i) + \lambda + \phi \tag{2.2}$$

In this system, only the direct charging and discharging will be taken into account. The term for indirect charging and discharging will be excluded, resulting in equation 2.3.

$$\frac{dT_i(t)}{dt} = \alpha \frac{T_{i+1} - 2T_i + T_{i-1}}{z^2} + \frac{K}{\rho c_p A}(T_\infty - T_i) + \frac{\dot{m}_i}{z \rho A}(T_i^{in} - T_i) + \lambda + \phi \tag{2.3}$$

Equation 2.3 still misses the effect of buoyancy and mixing. [17] has included these effects. The effect of slow buoyancy, the inversion of layers due to heat losses at the top of the tank as the top layer has a larger contact area to the tank, can be described with 2.4

$$\lambda = \theta_{i,i+1} \frac{1}{\mu} \log\left(e^0 + e^{\mu(T_{i+1} - T_i)}\right) - \theta_{i,i-1} \frac{1}{\mu} \log\left(e^0 + e^{\mu(T_i - T_{i-1})}\right) \tag{2.4}$$

where:

$$\theta_{i,i-1} = \frac{A_{i-1} z_{i-1}}{A_i z_i + A_{i-1} z_{i-1}} \in [0, 1] \tag{2.5}$$

Since it is assumed that all the layers have the same cross-sectional area and the same height, $\theta_{i,i-1}$ and $\theta_{i,i+1}$ can both be set to $\frac{1}{2}$. Furthermore, μ is used as a scaling factor to improve the formula depending on the storage type used [17]. [17] have found that an appropriate μ is equal to 10 for thermal storage vessels, resulting in equation 2.6.

$$\lambda = \frac{1}{20} \log\left(e^0 + e^{10(T_{i+1} - T_i)}\right) - \frac{1}{20} \log\left(e^0 + e^{10(T_i - T_{i-1})}\right) \tag{2.6}$$

Equations 2.2 and 2.6 can be combined into equation

$$\frac{dT_i(t)}{dt} = \alpha\frac{T_{i+1} - 2T_i + T_{i-1}}{z^2} + \frac{K}{\rho c_p A}(T_\infty - T_i) + \frac{\dot{m}_i}{z\rho A}(T_i - T_i^{in}) + \lambda \tag{2.7}$$

The mixing term is the only term missing from equation 2.7. This mixing term can be deduced from both [17] and [32], where they have included a step function, represented as $\mathrm{S}(T_i - T_l^{in})$, to check whether there is a temperature difference in each layer. This can be seen in 2.8 and 2.9, where $\dot{m}_i(T_i^{in} - T_i)$ from equation 2.7 is replaced by ϕ_1 and ϕ_2 into:

$$\phi_{1,i} = \tau\left(\dot{m}_1 S(T_i^{in} - T_i)(T_i^{in} - T_i) + \sum_{l=0}^{i} \dot{m}_1 \frac{(T_i - T_l^{in})S(T_i - T_l^{in})}{\sum_{j=l}^{N} S(T_j - T_l^{in})}\right), \text{if charging} \tag{2.8}$$

$$\phi_{2,i} = (1-\tau)\left(\dot{m}_n S(T_i - T_i^{in})(T_i^{in} - T_i) + \sum_{l=i}^{N} \dot{m}_n \frac{(T_l^{in} - T_i)S(T_l^{in} - T_i)}{\sum_{j=0}^{l} S(T_l^{in} - T_j)}\right), \text{if discharging} \tag{2.9}$$

Where

$$S(T_2 - T_1) = \begin{cases} 1, & \text{if } S(T_2 - T_1) \geq 0. \\ 0, & \text{otherwise.} \end{cases}$$

and

$$\tau = \begin{cases} 1, & \text{if charging.} \\ 0, & \text{discharging.} \end{cases}$$

Where the step function is approximated into a smooth and continuous function by [17], where [17] used [9, Chapter 11] for the approximation. Which looks like:

$$S(T_2 - T_1) \approx \frac{1}{1 + e^{-\eta(T_2 - T_1)}} \tag{2.10}$$

Where [17], found that an appropriate value of η is equal to 1. Both formulas 2.8 and 2.9 are artificial artifacts as they do not exactly describe the physics of mixing in a stratified thermal storage tank. The formula for charging checks whether the flow during charging is higher or equal to the temperature of the layers underneath (note that charging only happens in layer 1). If the incoming flow is higher than the temperature of the layers, it will charge the layer on which it flows, which is layer 1. If the temperature is lower than the temperature of one or more layers underneath, the temperature difference will be distributed equally between each layer. This also happens the other way around for discharging through layer 3. The equations 2.8 and 2.9 for the mixing can be combined with formula 2.7 into the complete ODE:

$$\frac{dT_i(t)}{dt} = \alpha\frac{T_{i+1} - 2T_i + T_{i-1}}{z^2} + \frac{K}{\rho c_p A}(T_\infty - T_i) + \frac{\phi_{1,i} + \phi_{2,i}}{z\rho A} + \lambda \tag{2.11}$$

This model needs to be written in matrix form to enable a state estimation strategy to estimate the temperature profile. The matrix form can be deduced from both [22] and [7] into a matrix with following structure:

$$\frac{dT}{dt} = AT + B + \phi_{\tau,i}\dot{m}$$

In this research, for simplicity reasons, only three layers will be used. However, to gain a clear insight on how the formula will work for n layers, n layers will be used in the following equations. Matrix A represents the heat flux given as:

$$A = \begin{bmatrix} -\alpha/z^2 - \frac{Pk}{\rho c_p A} & \alpha/z^2 & 0 & 0 & 0 \\ \alpha/z^2 & -2\alpha/z^2 - \frac{Pk}{\rho c_p A} & \alpha/z^2 & 0 & 0 \\ 0 & \alpha/z^2 & -2\alpha/z^2 - \frac{Pk}{\rho c_p A} & \ddots & 0 \\ 0 & 0 & \ddots & \ddots & \alpha/z^2 \\ 0 & 0 & 0 & \alpha/z^2 & -\alpha/z^2 - \frac{Pk}{\rho c_p A} \end{bmatrix}$$

Matrix B represents the slow buoyancy and part of the heat losses to the environment:

$$B = \begin{bmatrix} \frac{Pk}{\rho c_p A} T_\infty + \frac{1}{20} log(e^0 + e^{10(T_2 - T_1)} \\ \frac{P_2 k_2}{\rho c_p A} T_\infty + \frac{1}{20} \log\left(e^0 + e^{10(T_4 - T_3)}\right) - \frac{1}{20} \log\left(e^0 + e^{10(T_3 - T_2)}\right) \\ \vdots \\ \frac{P_n k_n}{\rho c_p A} T_\infty - \frac{1}{20} \log\left(e^0 + e^{10(T_n - T_{n-1})}\right) \end{bmatrix}$$

Matrix $\phi_{\tau,i}$ represents the mixing term for charging and discharging givens as:

$$\phi_{ch,i} = \begin{bmatrix} \frac{\phi_{1,1}}{z\rho A} + \frac{\phi_{2,1}}{z\rho A} \\ \frac{\phi_{1,2}}{z\rho A} + \frac{\phi_{2,2}}{z\rho A} \\ \vdots \\ \frac{\phi_{1,n}}{z\rho A} + \frac{\phi_{2,n}}{z\rho A} \end{bmatrix}$$

Where the $\phi_{1,i}$ and $\phi_{2,i}$ are defined the same as in formulas 2.8 and 2.9. These equations would look like formulas 2.12, 2.13, 2.14, 2.15, 2.16 and 2.17 in the matrix for i=1, i=2 and i=3 while taking working assumptions 5 and 6 into consideration; that the only inlet and outlet are coming from layers 1 and 3.

$$\begin{aligned} \phi_{1,1} =& \dot{m}_1 \frac{(T_1^{in} - T_1) S(T_1 - T_1^{in})}{S(T_1 - T_1^{in}) + S(T_2 - T_1^{in}) + S(T_3 - T_1^{in})} + \\ & \dot{m}_1 * S(T_1^{in} - T_1) * (T_1^{in} - T_1), \text{if charging} \end{aligned} \tag{2.12}$$

$$\begin{aligned} \phi_{1,2} =& \dot{m}_1 \frac{(T_1^{in} - T_2) S(T_2 - T_1^{in})}{S(T_1 - T_1^{in}) + S(T_2 - T_1^{in}) + S(T_3 - T_1^{in})} + \\ & \dot{m}_1 \frac{(T_2^{in} - T_2) S(T_2 - T_2^{in})}{S(T_2 - T_2^{in}) + S(T_3 - T_2^{in})} + \\ & \dot{m}_1 * S(T_2^{in} - T_2) * (T_2^{in} - T_2), \text{if charging} \end{aligned} \tag{2.13}$$

$$\begin{aligned} \phi_{1,3} =& \dot{m}_1 \frac{(T_1^{in} - T_3) S(T_3 - T_1^{in})}{S(T_1 - T_1^{in}) + S(T_2 - T_1^{in}) + S(T_3 - T_1^{in})} + \\ & \dot{m}_1 \frac{(T_2^{in} - T_3) S(T_3 - T_2^{in})}{S(T_2 - T_2^{in}) + S(T_3 - T_2^{in})} + \dot{m}_1 \frac{(T_3^{in} - T_3) S(T_3 - T_3^{in})}{S(T_3 - T_3^{in})} + \\ & \dot{m}_1 * S(T_3^{in} - T_3) * (T_3^{in} - T_3), \text{if charging} \end{aligned} \tag{2.14}$$

$$\phi_{2,1} = \dot{m}_3 \frac{(T_1^{in} - T_1)S(T_1^{in} - T_1)}{S(T_1^{in} - T_1)} + \dot{m}_3 \frac{(T_2^{in} - T_1)S(T_2^{in} - T_1)}{S(T_2^{in} - T_1) + S(T_2^{in} - T_2)} + \dot{m}_3 \frac{(T_3^{in} - T_1)S(T_3^{in} - T_1)}{S(T_3^{in} - T_1) + S(T_3^{in} - T_2) + S(T_3^{in} - T_3)} + \dot{m}_3 * (T_1^{in} - T_1)S(T_1 - T_1^{in}), \text{if discharging} \tag{2.15}$$

$$\phi_{2,2} = \dot{m}_3 \frac{(T_2^{in} - T_2)S(T_2^{in} - T_2)}{S(T_2^{in} - T_2) + S(T_2^{in} - T_1)} + \dot{m}_3 \frac{(T_3^{in} - T_2)S(T_3^{in} - T_2)}{S(T_3^{in} - T_1) + S(T_3^{in} - T_2) + S(T_3^{in} - T_3)} + \dot{m}_3 * (T_2^{in} - T_2)S(T_2 - T_2^{in}), \text{if discharging} \tag{2.16}$$

$$\phi_{2,3} = \dot{m}_3 \frac{(T_3^{in} - T_3)S(T_3^{in} - T_3)}{S(T_3^{in} - T_1) + S(T_3^{in} - T_2) + S(T_3^{in} - T_3)} + \dot{m}_3 * (T_3^{in} - T_3)S(T_3 - T_3^{in}), \text{if discharging} \tag{2.17}$$

2.3 Problem Formulation

The main problem in this paper is that there is no Sliding Mode Observer design yet for the temperature estimation of a stratified thermal storage tank in DHS applications. The objective is to review different Sliding Mode Observers, exploring whether they apply to the mathematical model described in this chapter. The Observer should comply to the following restraint

$$\lim_{t \to \infty} \hat{T} = T$$

For this review, first of all, literature research will be conducted. Secondly, after conducting research on the sliding mode technique and its ability to observe an unknown state, an analysis shall be carried out whether there is a variant of the sliding mode that applies to the modeled system as discussed in this chapter.

3 Bounded Disturbance Function for the Sliding Mode

3.1 Introduction to Sliding Mode Observers

This research shall look at the Sliding Mode Control technique as an observer for the system. The sliding mode technique is an advanced control method that has many applications for robust systems, as it can exclude both measurement noise and parameter uncertainty from the observer. Another important aspect is that the Sliding Mode technique allows finite-time convergence for all observable states [26].

According to [30], a sliding mode observer for a nonlinear system can be introduced to a system in the form of 3.1 when dealing with either parameter uncertainty, measurement noise, or both described by

$$\begin{aligned} \dot{T} &= AT + \Omega(T, \dot{m}) + Df(T, \dot{m}, t) \\ y &= CT \end{aligned} \tag{3.1}$$

where T, $\dot{m}$ and y are the state variables, input and output, respectively. In Sliding Mode Observer Design for nonlinear systems, there is an unknown error function consisting of uncertainties and noise given by $f(T, y, \dot{m}, t)$. For the sliding mode to work as an observer, it is required to design a bounded known disturbance function. The bounded disturbance function must comply with the constraint given in 3.2, where ψ is a function that needs to be designed [30].

$$||f(T, y, \dot{m}, t)|| \leq \psi(T, y, \dot{m}, t) \tag{3.2}$$

The disturbance function $\psi(T, y, \dot{m}, t)$ can be designed by looking into all possible parameters from system 2.11 and ascertain whether there might be an error present in the parameter.

3.2 Parameter Uncertainty

As shortly mentioned in the previous paragraph 3.1, to determine the known disturbance function $\psi(T, y, \dot{m}, t)$, all parameters must be analyzed for possible uncertainties or measurement noise. After each parameter is individually analyzed, the known disturbance function, ψ, can be designed. The disturbance function must be greater than, or equal to, the biggest possible unknown error function to ensure that the observer error can be driven to zero. Indicating that the disturbance function ψ is always equal to, or bigger than, each possible value of the unknown error described in system 3.1. The following paragraphs will look at each parameter to ascertain its possible uncertainty, if that applies to the parameter. Each parameter can be found in the nomenclature.

3.2.1 Thermal Conductivity (k)

The thermal conductivity of the insulation wall can be uncertain. According to [28], [15] and [34], the uncertainty for the thermal conductivity of a material is lower than 5 percent and mainly depends on the material, the thickness of the material, and the measurement technique. However, some other factors still play a role in the degree of uncertainty. If this research is to be expanded with a specific type of material and thickness, this percentage can be reduced to under 0.5 percent.

3.2.2 Density of Water (ρ)

The next parameter that has uncertainty is the density of water. The density of water is known per temperature, which only has an uncertainty of $1 * 10^{-6}$ [33], which is negligible in this research. However, the density is a nonlinear function with respect to the temperature. Since this nonlinear

function complicates the system, a constant value for all temperatures will be picked that will look like

$$\rho_{Tc} + \delta = \rho_{Ta}$$

where ρ_{Tc} and ρ_{Ta} are the densities for the chosen and actual temperature, respectively. The δ is the possible error. Since the tank will have boundaries for the temperature, which are T_{min} and T_{max} for the minimum and maximum temperature respectively, the maximum error δ can be calculated. The sliding mode technique can exclude the error from the function as long as it is bounded. Therefore, it is simpler to set the density to a constant with a bounded error function. Table 1 in appendix A [2] shows the density by temperature together. After determining T_{min} and T_{max}, a proper value for the density can be picked. In this research, the boundaries for T_{min} and T_{max} will be $0,01°C$ and $100°C$ respectively, as these boundaries are very unlikely to be exceeded. Furthermore, for all the parameters that are temperature dependent, namely fluid diffusivity, specific heat, and density, the value will be taken at $50°C$ as this is the exact temperature in-between the boundaries. In table 1, it can be seen that the maximum possible deviation with a constant $\rho = 988,04kg/m^3$ is $3,1\%$.

3.2.3 Specific Heat of Water

The third parameter that is not completely certain is the parameter for the specific heat of water. The specific heat capacity of a substance can be measured with differential scanning calorimetry [27], and [25]. Both [27] and [25] show that the uncertainty in these measurements will not exceed $1,5\%$. Besides this error, the Specific Heat of Water is also a nonlinear function with respect to the temperature of the water. The value from c_p will be picked at $50°C$, the same as for the density of water. The specific heat of water is different for isochoric (constant-volume) and isobaric (constant-pressure) circumstances. Working Assumption 8 shows that the volume of the tank stays constant. Therefore, the isochoric values are used in table 2 in Appendix A [3], which shows the values of c_p for each temperature. The third column shows the deviation from $c_p = 4,026 \ \ kJ/kg*T$, where the biggest deviation is at $T = 100°C$ and is equal to $6,85\%$ which will be rounded upwards to $6,9\%$. Combining this with the $1,5\%$ from the literature results in a total maximum error of $8,4\%$ for the specific heat capacity of water. Combining this with the error from subsections 3.2.2 and 3.2.1 will give the error

$$\begin{gathered}\text{Total Error } \rho,\ k \text{ and } c_p = 1,05/(1-0,031-0,084) = 1,19 \\ \psi(y,T,\dot{m},t) = (+/-)\left|0,19\frac{Pk}{\rho c_p A}(T_\infty - T_i)\right|\end{gathered} \tag{3.3}$$

3.2.4 Fluid Diffusivity

Fluid Diffusivity is a parameter that is dependent on thermal conductivity, specific heat, and density of water in the following way:

$$\alpha = \frac{k}{\rho c_p}$$

In the paragraphs about thermal conductivity, specific heat and density of water, their errors have already been determined as 5%; 8,4% and 3,1% with a total combined error at 19%

Furthermore, the fluid diffusivity is also nonlinear and dependent on the temperature, density, and specific heat capacity. The values for α can be found in table 3 in Appendix A [4] Beside this, the value for α is taken from $T = 50°C$ which equals to 0,155 * 10^{-6} m^2/s. The deviation per possible temperature is shown in the third column of table 3 and gives a value of $17,42\%$ rounding upwards gives $17,5\%$. Combining with the other part of the error results in $19 + 17,5 = 36,5\%$ error given by

$$\psi(y,T,\dot{m},t) = (+/-)\left|0,365 * \alpha\frac{T_{i+1} - 2T_i + T_{i-1}}{z^2}\right| \tag{3.4}$$

3.2.5 μ from the Slow Buoyancy

The μ from λ out of [17] is set at 10, which was found to be a reasonable value for heat storage vessels with a certain temperature difference between layers. In [17] they use temperatures between 5 and 85 $°C$, which is close to 20 percent outside of the range used in this paper, where the boundaries are $T \in (0,01; 100)$. Combined with the fact that μ is used to make the max function sharper, an error of 25 percent will be used in the error function.

This error cannot be incorporated in ψ like the other parameters since processing it as

$$\psi(y, T, \dot{m}, t) = \frac{1}{5}\log\left(e^0 + e^{2,5(T_{i+1}-T_i)}\right) - \frac{1}{5}\log\left(e^0 + e^{2,5(T_i-T_{i-1})}\right)$$

will result in the same value as the standard formula where μ is equal to 10. Therefore, in this situation, it is more accurate to include the error as 25% of the function for slow buoyancy itself by

$$\psi(y, T, \dot{m}, t) = 0,25 * \lambda_i \tag{3.5}$$

3.2.6 Eta from the mixing term

In the mixing term, the step function is approximated into a continuous function by formula 2.10 in chapter 2. This approximation has a parameter η that helps fabricate a rigorous formula. In [17], they take a value of 1, which works for their model and simulations. However, it is complicated to examine whether this parameter is even close to the correct number for this research. If η is gaining steeper, the approximation becomes more accurate by design. However, this does not imply directly that it also produces a more precise formula in this application. This research focuses on parameter uncertainty and measurement noise, not on parameter design. Therefore, an upper and a lower bound are set for η by

$$\eta^{min} \leq \eta \leq \eta^{max} \quad \text{where} \quad \eta^{min} = 0,5\eta \wedge \eta^{max} = 1,5\eta$$

This is incorporated in the disturbance by

$$\phi_{1,i} = \tau\left(\dot{m}_1 \frac{1}{1+e^{-0,5(T_i^{in}-T_i)}}(T_i^{in}-T_i) + \sum_{l=0}^{i}\dot{m}_1 \frac{(T_i - T_l^{in})\frac{1}{1+e^{-0,5(T_i-T_l^{in}))}}}{\sum_{j=l}^{N}\frac{1}{1+e^{-0,5(T_j-T_l^{in}))}}}\right), \text{if charging} \tag{3.6}$$

$$\phi_{2,i} = (1-\tau)\left(\dot{m}_n * \frac{1}{1+e^{-0,5(T_i-T-_i^{in})}}(T_i^{in}-T_i) + \sum_{l=i}^{N}\dot{m}_n \frac{(T_l^{in}-T_i)\frac{1}{1+e^{-0,5(T_l^{in}-T_i))}}}{\sum_{j=0}^{l}\frac{1}{1+e^{-0,5(T_l^{in}-T_j))}}}\right), \text{if discharging} \tag{3.7}$$

since the bounds are equal to 50% of η.

3.2.7 Remaining Parameters

The parameters that do not contain error or measurement noise are: the thickness of the layer z, the perimeter of the layers P, the cross-sectional area of the layers A and theta θ in λ as it is only dependent on A and z.

3.3 Measurement Noise / Uncertainty

In the following paragraphs, the possible noise from measurements and uncertainty in the sensors will be discussed so that it can be used in the bounded disturbance function.

3.3.1 Measured Mass Flow Rate

The mass flow rate has $\dot{m}_i$ has an impact on the mixing term $\phi_{i,i}$. According to [12], the kinetic differential pressure method is a method that is better accessible than direct measurement, magnetic flow meters or ultra-sonic flow meters, due to lesser boundaries to the system, such as restrictions in flow rate changes and (isolation)material of the pipe. In [13], the error does not exceed 2%, but in [12], the average error was in the order of $0,1\%$, with a maximum error of $6,41\%$, which can be rounded upwards for the boundary of the disturbance system to $6,5\%$.

3.3.2 Measured Temperature and Temperature of the Inflow

There are a lot of different methods for measuring the temperature of a fluid [6]. Depending on the method, a valid error can be found. If the temperature were to be measured with either: Platinum resistance thermometers, thermistors, or semiconductor devices, the error would be maximum $\pm 1°C$ for commercial applications [6]. This will be rounded upwards to $2°C$ ensuring that it is adequately bounded.

3.4 Disturbance Function

All the uncertainties in the parameters and the measurement noise or deviation have been determined, allowing the complete bounded disturbance formula to be compiled. Combining the maximum errors from (ref all the paragraphs here) into

$$\begin{aligned}\psi(y,T,\dot{m},t) = \pm\Bigg(&\left|0,365 * \alpha\frac{T_{i+1}-2T_i+T_{i-1}}{z^2}\right| + \left|0,19\frac{Pk}{\rho c_p A}(T_\infty - T_i)\right| \\ &+\left|0,25*\lambda\right| + \left|\frac{0,065\phi_{a1,i}}{\rho c_p A} + \frac{0,065\phi_{a2,i}}{\rho c_p A}\right| + \left|\frac{\phi_{b1,i}}{\rho c_p A} + \frac{\phi_{b2,i}}{\rho c_p A}\right|\Bigg)\end{aligned} \tag{3.8}$$

where

$$\phi_{a1,i} = \tau\left(\dot{m}_1\frac{1}{1+e^{-(T_i^{in}-T_i)}}(T_i^{in}-T_i) + \sum_{l=0}^{i}\dot{m}_1\frac{(T_i-T_l^{in})\frac{1}{1+e^{-(T_i-T_l^{in}))}}}{\sum_{j=l}^{N}\frac{1}{1+e^{-(T_j-T_l^{in}))}}}\right), \text{if charging} \tag{3.9}$$

$$\phi_{a2,i} = (1-\tau)\left(\dot{m}_n * \frac{1}{1+e^{-(T_i-T-_i^{in})}}(T_i^{in}-T_i) + \sum_{l=i}^{N}\dot{m}_n\frac{(T_l^{in}-T_i)\frac{1}{1+e^{-(T_l^{in}-T_i))}}}{\sum_{j=0}^{l}\frac{1}{1+e^{-(T_l^{in}-T_j))}}}\right), \text{if discharging} \tag{3.10}$$

$$\phi_{b1,i} = \tau\left(\dot{m}_1\frac{1}{1+e^{-0,5(T_i^{in}-T_i)}}(T_i^{in}-T_i) + \sum_{l=0}^{i}\dot{m}_1\frac{(T_i-T_l^{in})\frac{1}{1+e^{-0,5(T_i-T_l^{in}))}}}{\sum_{j=l}^{N}\frac{1}{1+e^{-0,5(T_j-T_l^{in}))}}}\right), \text{if charging} \tag{3.11}$$

$$\phi_{b2,i} = (1-\tau)\left(\dot{m}_n * \frac{1}{1+e^{-0,5(T_i-T-_i^{in})}}(T_i^{in}-T_i) + \sum_{l=i}^{N}\dot{m}_n\frac{(T_l^{in}-T_i)\frac{1}{1+e^{-0,5(T_l^{in}-T_i))}}}{\sum_{j=0}^{l}\frac{1}{1+e^{-0,5(T_l^{in}-T_j))}}}\right), \text{if discharging} \tag{3.12}$$

Formula 3.8 shows the disturbance for layer i, whereas formula 3.13 shows the total disturbance for each layer by

$$\psi(y,T,\dot{m},t) = \pm \begin{bmatrix} -0,365\alpha/z^2 & 0,365\alpha & 0 \\ 0,365\alpha & -2*0,365\alpha/z^2 & 0,365\alpha \\ 0 & 0,365\alpha & -2*0,365\alpha/z^2 \end{bmatrix} \begin{bmatrix} T_1 \\ T_2 \\ T_3 \end{bmatrix} \tag{3.13}$$

$$+ \begin{bmatrix} \frac{0,19P_1k_1}{\rho c_p A} & 0 & 0 \\ 0 & \frac{0,19P_2k_2}{\rho c_p A} & 0 \\ 0 & 0 & \frac{0,19P_nk_n}{\rho c_p A} \end{bmatrix} \begin{bmatrix} T_\infty - T_1 \\ T_\infty - T_2 \\ T_\infty - T_3 \end{bmatrix} \tag{3.14}$$

$$+0,25* \begin{bmatrix} \frac{1}{20} log(e^0 + e^{10(T_2-T_1)}) \\ \frac{1}{20}\log\left(e^0 + e^{10(T_3-T_2)}\right) - \frac{1}{20}\log\left(e^0 + e^{10(T_2-T_1)}\right) \\ -\frac{1}{20}\log\left(e^0 + e^{10(T_3-T_2)}\right) \end{bmatrix} \tag{3.15}$$

$$+ \begin{bmatrix} \frac{0,065\dot{m}_1}{\rho c_p A}\tau \left(\dot{m}_1 \frac{1}{1+e^{-(T_1^{in}-T_1)}}(T_1^{in}-T_1) + \sum_{l=0}^{1} \dot{m}_1 \frac{(T_i - T_l^{in})\frac{1}{1+e^{-(T_i-T_l^{in}))}}}{\sum_{j=l}^{N} \frac{1}{1+e^{-(T_j-T_l^{in}))}}} \right) \\ \frac{0,065\dot{m}_1}{\rho c_p A}\tau \left(\dot{m}_1 \frac{1}{1+e^{-(T_2^{in}-T_2)}}(T_2^{in}-T_2) + \sum_{l=0}^{2} \dot{m}_1 \frac{(T_i - T_l^{in})\frac{1}{1+e^{-(T_i-T_l^{in}))}}}{\sum_{j=l}^{N} \frac{1}{1+e^{-(T_j-T_l^{in}))}}} \right) \\ \frac{0,065\dot{m}_1}{\rho c_p A}\tau \left(\dot{m}_1 \frac{1}{1+e^{-(T_3^{in}-T_3)}}(T_3^{in}-T_3) + \sum_{l=0}^{3} \dot{m}_1 \frac{(T_i - T_l^{in})\frac{1}{1+e^{-(T_i-T_l^{in}))}}}{\sum_{j=l}^{N} \frac{1}{1+e^{-(T_j-T_l^{in}))}}} \right) \end{bmatrix} \tag{3.16}$$

$$+ \begin{bmatrix} \frac{0,065\dot{m}_1}{\rho c_p A}(1-\tau) \left(\dot{m}_n * \frac{1}{1+e^{-(T_1-T-\frac{in}{i}_1)}}(T_1^{in}-T_1) + \sum_{l=1}^{N} \dot{m}_n \frac{(T_l^{in} - T_i)\frac{1}{1+e^{-(T_l^{in}-T_i))}}}{\sum_{j=0}^{l} \frac{1}{1+e^{-(T_l^{in}-T_j))}}} \right) \\ \frac{0,065\dot{m}_1}{\rho c_p A}(1-\tau) \left(\dot{m}_n * \frac{1}{1+e^{-(T_2-T-\frac{in}{2})}}(T_2^{in}-T_2) + \sum_{l=2}^{N} \dot{m}_n \frac{(T_l^{in} - T_i)\frac{1}{1+e^{-(T_l^{in}-T_i))}}}{\sum_{j=0}^{l} \frac{1}{1+e^{-(T_l^{in}-T_j))}}} \right) \\ \frac{0,065\dot{m}_1}{\rho c_p A}(1-\tau) \left(\dot{m}_n * \frac{1}{1+e^{-(T_3-T-\frac{in}{3})}}(T_3^{in}-T_3) + \sum_{l=3}^{N} \dot{m}_n \frac{(T_l^{in} - T_i)\frac{1}{1+e^{-(T_l^{in}-T_i))}}}{\sum_{j=0}^{l} \frac{1}{1+e^{-(T_l^{in}-T_j))}}} \right) \end{bmatrix}$$

$$+ \begin{bmatrix} \frac{\dot{m}_1}{\rho c_p A}\tau \left(\dot{m}_1 \frac{1}{1+e^{-0,5(T_1^{in}-T_1)}}(T_1^{in}-T_1) + \sum_{l=0}^{1} \dot{m}_1 \frac{(T_i - T_l^{in})\frac{1}{1+e^{-0,5(T_i-T_l^{in}))}}}{\sum_{j=l}^{N} \frac{1}{1+e^{-0,5(T_j-T_l^{in}))}}} \right) \\ \frac{\dot{m}_1}{\rho c_p A}\tau \left(\dot{m}_1 \frac{1}{1+e^{-0,5(T_2^{in}-T_2)}}(T_2^{in}-T_2) + \sum_{l=0}^{2} \dot{m}_1 \frac{(T_i - T_l^{in})\frac{1}{1+e^{-0,5(T_i-T_l^{in}))}}}{\sum_{j=l}^{N} \frac{1}{1+e^{-0,5(T_j-T_l^{in}))}}} \right) \\ \frac{\dot{m}_1}{\rho c_p A}\tau \left(\dot{m}_1 \frac{1}{1+e^{-0,5(T_3^{in}-T_3)}}(T_3^{in}-T_3) + \sum_{l=0}^{3} \dot{m}_1 \frac{(T_i - T_l^{in})\frac{1}{1+e^{-0,5(T_i-T_l^{in}))}}}{\sum_{j=l}^{N} \frac{1}{1+e^{-0,5(T_j-T_l^{in}))}}} \right) \end{bmatrix} \tag{3.17}$$

$$+ \begin{bmatrix} \frac{\dot{m}_1}{\rho c_p A}(1-\tau) \left(\dot{m}_n * \frac{1}{1+e^{-0,5(T_1-T-\frac{in}{1})}}(T_1^{in}-T_1) + \sum_{l=1}^{N} \dot{m}_n \frac{(T_l^{in} - T_i)\frac{1}{1+e^{-0,5(T_l^{in}-T_i))}}}{\sum_{j=0}^{l} \frac{1}{1+e^{-0,5(T_l^{in}-T_j))}}} \right) \\ \frac{\dot{m}_1}{\rho c_p A}(1-\tau) \left(\dot{m}_n * \frac{1}{1+e^{-0,5(T_2-T-\frac{in}{2})}}(T_2^{in}-T_2) + \sum_{l=2}^{N} \dot{m}_n \frac{(T_l^{in} - T_i)\frac{1}{1+e^{-0,5(T_l^{in}-T_i))}}}{\sum_{j=0}^{l} \frac{1}{1+e^{-0,5(T_l^{in}-T_j))}}} \right) \\ \frac{\dot{m}_1}{\rho c_p A}(1-\tau) \left(\dot{m}_n * \frac{1}{1+e^{-0,5(T_3-T-\frac{in}{3})}}(T_3^{in}-T_3) + \sum_{l=3}^{N} \dot{m}_n \frac{(T_l^{in} - T_i)\frac{1}{1+e^{-0,5(T_l^{in}-T_i))}}}{\sum_{j=0}^{l} \frac{1}{1+e^{-0,5(T_l^{in}-T_j))}}} \right) \end{bmatrix}$$

which shows a linear part in the first two terms 3.13 3.14,and a nonlinear part in the second three terms 3.15 3.16 3.17.

4 Review of Sliding Mode Observers

4.1 Basic Introduction to the Sliding Mode

In control systems, there are almost always discrepancies between the plant and the mathematical model that is developed for either the controller or the observer. This can come from very complex physical models that are simplified or from parameters. For these kinds of systems, robust control is critical. The Sliding Mode methodology is one of such robust control methods. The sliding mode uses an introduced variable that is part of the system, namely the sliding surface. The sliding surface can be seen as a line in the system's phase portrait, shown in figure 3. First, a control drives the system towards the sliding surface $\mathcal{S}$; this is called the reaching mode. When the system is on the trajectory of the sliding surface, a discontinuous signal is applied to drive the system toward zero, called the sliding mode. During the sliding mode, the difference between the mathematical model and the plant will be driven to zero. During the sliding mode, the system is independent of possible bounded uncertainties or disturbances, making it a strong, robust control method.

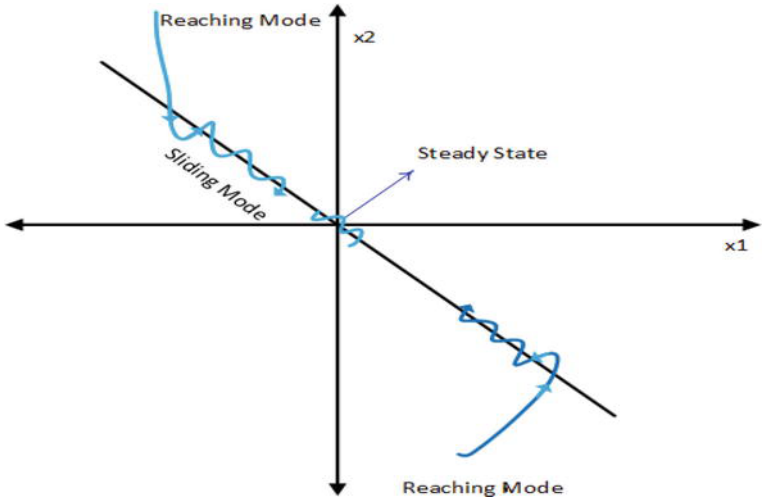

Figure 3: *The trajectory of the sliding mode [29]*

4.2 Linear System without disturbances

The book of [30] describes all types of observers for systems. The system can be first-order, higher-order, linear or nonlinear, with or without disturbances. The coming sections will extensively go through sliding mode observers for the system in chapter 2, to offer a precise comprehension of the reasoning and functioning of sliding mode observers. Note that all the following explanations (sections 4.2, 4.3, 4.4 , 4.5) are deducted from the book of [30].

For a first order linear system with no disturbances, considered by the altered system from chapter 2

$$\begin{aligned} \dot{T}_i(t) &= AT_i(t) + B\dot{m}(t) \\ y(t) &= CT(t) \end{aligned} \tag{4.1}$$

where A $\in \mathbb{R}^{n\times n} \rightarrow$ A $\in \mathbb{R}^{3\times 3}$, B $\in \mathbb{R}^{n\times m} \rightarrow$ B $\in \mathbb{R}^{3\times 3}$ and C $\in \mathbb{R}^{p\times n} \rightarrow$ C $\in \mathbb{R}^{2\times 3}$. Where matrix C has full row rank, meaning that all the measured outputs are independent, which is true since

$$C = \begin{bmatrix} 1 & 0 & 0 \\ 0 & 0 & 1 \end{bmatrix} \tag{4.2}$$

which has this form due to the measured states T_1 and T_3(see working assumption 5). Furthermore, the duo (A,C) must be observable.

The first step for designing a sliding mode observer is creating a coordinate transformation of the initial system 4.1. The transformation will have the following form

$$T_c = \begin{bmatrix} N_c^T \\ C \end{bmatrix} \rightarrow \begin{bmatrix} 0 & 1 & 0 \\ 1 & 0 & 0 \\ 0 & 0 & 1 \end{bmatrix} \tag{4.3}$$

this transformation will be applied to the triple (A,B,C) and realizes one very important aspect for the observer, as it will allow the error function to be split in both e and e_y (this will be shown later in the explanation of equations 4.12 and 4.13). The observer will have the form

$$\begin{aligned} \dot{\hat{T}}(t) &= A\hat{T}(t) + B\dot{m}(t) + G_n v \\ \hat{y}(t) &= C\hat{T}(t) \end{aligned} \tag{4.4}$$

where matrix B is applicable on the input, however, the input is still nonlinear as described by 2.8, 2.9 and 2.10. However, since this is a sliding mode observer for a linear system (4.1), the input should be linearized using a Jacobian Matrix. The matrix coordinates in equation 4.4 are assumed to already be linearized and in the following form

$$A = T_c A T_c^{-1} = \begin{bmatrix} A_{11} & A_{12} \\ A_{21} & A_{22} \end{bmatrix}, \quad B = T_c B = \begin{bmatrix} B_1 \\ B_2 \end{bmatrix} \quad \text{and } CT_c^{-1} = \begin{bmatrix} 0 & I_p \end{bmatrix} \tag{4.5}$$

where $(\hat{x}, \hat{y})$ are the state estimates of (x, y). Furthermore, the v is the discontinuous injection term that is defined per layer i as

$$v_i = \beta \text{sign}(e_{y,i}), \quad \beta = \text{a positive scalar}$$

This term is designed to force e(t) to the sliding surface $\mathcal{S} = \{\text{e} : \text{Ce=0}\}$ in finite time as the term is discontinuous with respect to $\mathcal{S}$. Assuming the system is already in the form of 4.5, the gain G_n is designed as

$$G_n = \begin{bmatrix} L \\ -I_p \end{bmatrix} \tag{4.6}$$

where $-I_p$ is defined as the negative identity matrix with size p and $\text{L} \in \mathbb{R}^{n-p \times p}$ is free for design. The errors for the state and the output are defined by

$$e(t) = \hat{T}(t) - T(t) \tag{4.7}$$

$$e_y(t) = \hat{y}(t) - y(t) \tag{4.8}$$

and where the derivative of the system, error $\dot{e}(t)$, is defined by

$$\dot{e}(t) = \dot{\hat{T}}(t) - \dot{T}(t) \tag{4.9}$$

$$= (A\hat{T}(t) + B\dot{m}(t) + G_n v) - (AT_i(t) + B\dot{m}_i(t)) \tag{4.10}$$

$$= Ae(t) + G_n v \tag{4.11}$$

this is where the important aspect from the coordinate transformation comes into play, as the error function $e_y(t)$ is defined by

$$\begin{aligned} e_y(t) &= \hat{y}(t) - y(t) \\ &= C(\hat{T}(t) - T(t)) \\ &= Ce(t) \\ &= \begin{bmatrix} 0 & I_p \end{bmatrix} e(t) \end{aligned}$$

showing that the error of the output $e_y(t)$ consists of the last p terms of the error of the state e. This induces a possible split of the error function of the state into both a function of e as of e_y and is partitioned as $e = col(e_1, e_y)$ and the error system can thus be described as

$$\dot{e_1}(t) = A_{11}e(t) + A_{12}e_y(t) + Lv \tag{4.12}$$
$$\dot{e_y}(t) = A_{21}e(t) + A_{22}e_y(t) - v \tag{4.13}$$

where $\dot{e_y}(t)$ can be divided into layers as

$$\dot{e_{y,i}}(t) = A_{21,i}e(t) + A_{22,i}e_y(t) - \beta sign(e_{y,i} \tag{4.14}$$

To achieve asymptotic convergence of the state, firstly the error $e_y(t)$ must be driven to zero in finite time. This can be achieved by introducing a candidate Lyapunov function (See Appendix B for Lyapunov Stability) in the form of:

$$V = \frac{1}{2}e_y^2 \tag{4.15}$$

where the derivative of the Lyapunov function is defined by

$$\dot{V} = \dot{e_y}e_y \tag{4.16}$$

ensuring that equation 4.13 is asymptotically stable results in two conditions that must be satisfied, namely:

1. $\dot{V} < 0$ for $e_y(t) \neq 0$
2. For $e_y(t) \to \infty$, V $\to \infty$

where the second condition is satisfied, as can be seen directly from equation 4.15. The first condition can be stated as

$$\dot{e_{y,i}}e_{y,i} = e_{y,i}\Big(A_{21,i}e_1 + A_{22,i}e_y - \beta sign(e_{y,i})\Big) \tag{4.17}$$
$$= e_{y,i}\Big(A_{21,i}e_1 + A_{22,i}e_y\Big) - \beta|e_{y,i}| \tag{4.18}$$
$$< -|e_{y,i}|\ (\beta - |(A_{21,i}e_1 + A_{22,i}e_y)|) \tag{4.19}$$

where the step from equation 4.17 to 4.18 follows from the fact that $x * sign(x) = |x|$. Scalar β must also comply to the following constraint in order for the equation to hold:

$$\beta > |A_{21,i}e_1 + A_{22,i}e_y| + \kappa \tag{4.20}$$

where the scalar κ complies to $\kappa \in \mathbb{R}_+$, otherwise, equation 4.18 could be positive and would thus violate the first condition for the asymptotic stability of the Lyapunov candidate. This will result in the final "reachability" condition

$$\dot{e_{y,i}}e_{y,i} < \kappa|e_{y,i}| \tag{4.21}$$

If equation 4.21 holds, the error $e_{y,i}$ will converge to zero in finite time and subsequently a sliding mode takes place on $\mathcal{S}$. During this sliding motion, both errors e_1 and e_y are zero and the systems 4.12 and 4.13 can be described as

$$\dot{e_1}(t) = A_{11}e(t) + Lv_{eq} \tag{4.22}$$
$$0 = A_{21}e(t) - v_{eq} \tag{4.23}$$

where v_{eq} is the equivalent output error injection which is required to maintain the sliding motion. Equation 4.23 shows that

$$v_{eq} = A_{21}e(t) \tag{4.24}$$

which can be substituted into 4.22 resulting in

$$\dot{e_1}(t) = (A_{11}(t) + LA_{21}(t))e_1(t) \tag{4.25}$$

this represent the reduced order motion governing the sliding motion and is of size: (n-p), as can be deducted from the sizes as discussed after equation 4.1 and the coordinate transformation 4.5. L represents total freedom of design for the observer, and can thus always assure that 4.25 is stable. This shows how a very simplistic sliding mode observer would reconstruct the unknown states of a linear system.

4.3 Linear system with disturbances

Now a linear system with some disturbance will be discussed, looking at the possibility of reconstructing the unknown states when there is an unknown disturbance in the system. System 4.1 from the previous chapter can be replaced with

$$\begin{aligned} \dot{T}_i(t) &= AT_i(t) + B\dot{m}(t) + D\xi(T, \dot{m}, t) \\ y(t) &= CT(t) \end{aligned} \tag{4.26}$$

where D is the distribution matrix $\in \mathbb{R}^{p\times h}$ of the associated disturbance described by $\xi(T, \dot{m}, t) \in \mathbb{R}^h$. The gain G_n is in the new system desired to match the disturbance D, such that D = G_nX, where X is free to be designed, as long as $X \in \mathbb{R}^{p\times h}$ combining this with the coordinate transformation and the design of G_n:

$$A = T_c A T_c^{-1} = \begin{bmatrix} A_{11} & A_{21} \\ A_{21} & A_{22} \end{bmatrix}, \quad B = T_c B = \begin{bmatrix} B_1 \\ B_2 \end{bmatrix}, \; CT_c^{-1} = \begin{bmatrix} 0 & I_p \end{bmatrix} \text{ and } G_n = \begin{bmatrix} L \\ -I_p \end{bmatrix} \tag{4.27}$$

results in matrix D

$$D = G_n X = \begin{bmatrix} L \\ -I_p \end{bmatrix} X \tag{4.28}$$

This form of D is fundamental for the error dynamics that will follow from this. The error dynamics can be shown in the same way as in the previous chapter, namely as:

$$\dot{e}(t) = \hat{\dot{T}}(t) - \dot{T}(t) \tag{4.29}$$

$$= (A\hat{T}(t) + B\dot{m}(t) + G_n v) - (AT_i(t) + B\dot{m}_i(t) + D\xi(T, \dot{m}, t)) \tag{4.30}$$

$$= Ae(t) + G_n v - D\xi(T, \dot{m}, t) \tag{4.31}$$

this error can once again be split up into $e_1(t)$ and $e_y(t)$ since the essential system dynamic of the coordinate transformation remains equal to the linear version. The error can be partitioned again as e = col(e_1, e_y) and the derived error can thus be described as

$$\dot{e_1}(t) = A_{11}e_1(t) + A_{21}e_y(t) + Lv - LX\xi(T, \dot{m}, t) \tag{4.32}$$

$$\dot{e_y}(t) = A_{21}e_1(t) + A_{21}e_y(t) - v + X\xi(T, \dot{m}, t) \tag{4.33}$$

due to the design of $D = G_n X$. When $e_y(t)$ is driven to zero with a slightly different reachability condition than for the linear system (shown in equation 4.40), the error dynamics will look like

$$\dot{e_1}(t) = A_{11}e_1(t) + Lv_{eq} - LX\xi(T, \dot{m}, t) \tag{4.34}$$

$$0 = A_{21}e_1(t) - v_{eq} + X\xi(T, \dot{m}, t) \tag{4.35}$$

the charm in the design of $D = G_n X$ really shows here, as v_eq can be substituted into $\dot{e_1}(t)$ by

$$v_{eq} = A_{21}e_1(t) + X\xi(T, \dot{m}, t) \tag{4.36}$$

$$\dot{e_1}(t) = A_{11}e_1(t) + Lv_{eq} - LX\xi(T, \dot{m}, t) \tag{4.37}$$

$$\dot{e_1}(t) = A_{11}e_1(t) + L(A_{21}e_1(t) + X\xi(T, \dot{m}, t)) - LX\xi(T, \dot{m}, t) \tag{4.38}$$

$$= (A_{11} + LA_{21})e_1(t) \tag{4.39}$$

which is completely independent of the disturbance $\xi(T, \dot{m}, t)$ due to the coordinate transformation and design of the disturbance matrix M. However, before L can be designed, the reachability condition needs to be developed again for the system dynamics with disturbance. This can be performed the same way as in the previous chapter by designing a candidate Lyapunov function that must comply to the two conditions 4.2. This will result in

$$\begin{aligned} \dot{e_{y,i}} e_{y,i} &= e_{y,i}\Big(A_{21,i}e_1 + A_{22,i}e_y + X_i\xi - \beta sign(e_{y,i})\Big) \\ &= e_{y,i}\Big(A_{21,i}e_1 + A_{22,i}e_y + X_i\xi\Big) - \beta|e_{y,i}| \\ &< -|e_{y,i}|\left(\beta - |(A_{21,i}e_1 + A_{22,i}e_y + X_i\xi(T, \dot{m}, t))|\right) \end{aligned} \tag{4.40}$$

where the scalar β must also comply to the following constraint in order for the equation to hold:

$$\beta > |A_{21,i}e_1 + A_{22,i}e_y + X_i\xi(T, \dot{m}, t)| + \kappa \tag{4.41}$$

where $\kappa \in \mathbb{R}_+$.

However, in paragraph 3.4 detailing the error function, it can be seen that the bounded error function consists of each layer. Therefore, matrix D of the error function $\xi(T, \dot{m}, t)$ must consist of an identity matrix, otherwise the output of the disturbance will not affect each layer as it is supposed to. This takes away the design freedom for matrix L completely and will not result in

$$D = G_n X = \begin{bmatrix} L \\ -I_p \end{bmatrix} X \tag{4.42}$$

which is fundamental for the design of the observer. This shows that it is not possible to observe the linear 1-dimensional model of a stratified thermal storage tank when there is noise and parameter uncertainty present in each layer of the tank.

4.4 Nonlinear system with disturbances

It is still important to check whether the sliding mode could be applied as an observer to the mathematical model developed in chapter 2, as that model is nonlinear and can be described as

$$\dot{T_i} = AT_i + B(\dot{m}, T) + D\xi(T, \dot{m}, t) \tag{4.43}$$

$$y = CT \tag{4.44}$$

where $T \in \mathbb{R}^n$, $\dot{m} \in \mathbb{R}^m$ and $y \in \mathbb{R}^p$ are the state variables, inputs and outputs respectively. And $A \in \mathbb{R}^{n\times n}$, D $\in \mathbb{R}^{n\times q}$ and $C \in \mathbb{R}^{p\times n}$. One very important constraint for this system is $n > p \geq q$. This constraint will allow part of the gain L to be designed with a certain freedom later on in designing the observer. Breaking this constraint would result in zero degree of freedom for the observer design. This would obviously prevent the design of the whole observer. Therefore, it is not possible to design a sliding mode observer, either linear or nonlinear, for the 1-dimensional mathematical model as depicted in this research.

4.5 Realizing a narrowed-down Sliding Mode Observer

In the previous paragraphs, the sliding mode is discussed step for step and it shows that with the current model, it is impossible to apply the sliding mode method. Within the linear variant with disturbances, the matrix G_n cannot be designed due to properties of the error function D. For the nonlinear variant, the dimensions of the error function violate the first constraint. However, it is possible to avoid these problems by proposing some changes to the error dynamics and corresponding matrix. The changed error matrix and dynamics would not contain the complete error function, but only the conduction and the slow buoyancy terms and would look like

$$\omega(T, y) = D \begin{bmatrix} \frac{0{,}365\alpha}{z^2} * (T_2 - T_1) + \frac{1}{4}\frac{1}{20} log(e^0 + e^{10(T_2 - T_1)}) \\ \frac{0{,}365\alpha}{z^2} * (T_2 - T_3) - \frac{1}{4}\frac{1}{20} log(e^0 + e^{10(T_3 - T_2)}) \end{bmatrix} \tag{4.45}$$

with matrix D

$$D = \begin{bmatrix} 1 & 0 \\ -1 & -1 \\ 0 & 1 \end{bmatrix} \tag{4.46}$$

which will result in the same output for the conduction slow buoyancy and as in the complete error function $\psi(y, T, \dot{m}, t)$ as using the identity matrix due to the interconnection of the terms in each layer, shown by

$$\omega(T, y) = \begin{bmatrix} 1 & 0 \\ -1 & -1 \\ 0 & 1 \end{bmatrix} \begin{bmatrix} \frac{0{,}365\alpha}{z^2} * (T_2 - T_1) + \frac{1}{80} log(e^0 + e^{10(T_2 - T_1)}) \\ \frac{0{,}365\alpha}{z^2} * (T_2 - T_3) - \frac{1}{80} log(e^0 + e^{10(T_3 - T_2)}) \end{bmatrix} \tag{4.47}$$

$$= \begin{bmatrix} \frac{0{,}365\alpha}{z^2} * (T_2 - T_1) + \frac{1}{80} log(e^0 + e^{10(T_2 - T_1)}) \\ \frac{0{,}365\alpha}{z^2} * ((T_3 - T_2) - (T_2 - T_1)) + \frac{1}{80} log\left(\frac{e^0 + e^{10(T_3 - T_2)}}{e^0 + e^{10(T_2 - T_1)}}\right) \\ \frac{0{,}365\alpha}{z^2} * (T_2 - T_3) - \frac{1}{80} log(e^0 + e^{10(T_3 - T_2)}) \end{bmatrix} \tag{4.48}$$

with this error construction, it is possible to design an observer using the sliding mode, as long as the regular assumptions for the observer design are met. A large flaw is that the error of the ambient temperature and the error of the mixing terms cannot be taken into account with this error structure, as those errors cannot be constructed in a similar manner.

Due to the changes in the error function and corresponding matrix D, it is now more likely that an observer design might be possible. This could possibly be designed for both a linear as a nonlinear system. However, the design for a nonlinear system will take more time and knowledge, which is not possible within the time scope of this research. Therefore, the current system will be linearized with help of Jacobian Matrices, in order to enable the possibility of simulations further on in this research. The nonlinear system looks like

$$\frac{dT}{dt} = AT + B + C + \phi + D\omega(T, y) \tag{4.49}$$

$$= \begin{bmatrix} -\frac{a}{z^2} - \frac{Pk}{\rho c_p A} & \frac{a}{z^2} & 0 \\ \frac{a}{z^2} & -2\frac{a}{z^2} - \frac{Pk}{\rho c_p A} & \frac{a}{z^2} \\ 0 & \frac{a}{z^2} & -\frac{a}{z^2} - \frac{Pk}{\rho c_p A} \end{bmatrix} \begin{bmatrix} T_1 \\ T_2 \\ T_3 \end{bmatrix} \tag{4.50}$$

$$+ \begin{bmatrix} \frac{1}{20} log(e^0 + e^{10(T_2 - T_1)}) \\ \frac{1}{20} log(e^0 + e^{10(T_3 - T_2)}) - \frac{1}{20} log(e^0 + e^{10(T_2 - T_1)}) \\ \frac{1}{20} log(e^0 + e^{10(T_3 - T_2)}) \end{bmatrix} + \begin{bmatrix} \frac{Pk}{\rho c_p A} T_\infty \\ \frac{Pk}{\rho c_p A} T_\infty \\ \frac{Pk}{\rho c_p A} T_\infty \end{bmatrix} \tag{4.51}$$

$$+ \begin{bmatrix} \frac{\phi_{1,1}}{z\rho A} + \frac{\phi_{2,1}}{z\rho A} \\ \frac{\phi_{1,2}}{z\rho A} + \frac{\phi_{2,2}}{z\rho A} \\ \frac{\phi_{1,3}}{z\rho A} + \frac{\phi_{2,3}}{z\rho A} \end{bmatrix} + D\omega(T, y) \tag{4.52}$$

where the nonlinearity's are in the second matrix, B, where the slow buoyancy is the nonlinearity, and in the third matrix, $\phi_{ch,i}$, where the mixing term is the nonlinearity. These functions can be

linearized with a Jacobion Matrix, which would generally look like:

$$\frac{dT}{dt} = \left(A + \frac{\partial B}{\partial T}\bigg|_{T=\bar{T}} + \frac{\partial C}{\partial T}\bigg|_{T=\bar{T}} \right) T + \frac{\partial C}{\partial \dot{m}}\bigg|_{\substack{T=\bar{T} \\ \dot{m}=\bar{m}}} \dot{m} \tag{4.53}$$

$$- \left(\frac{\partial B}{\partial T}\bigg|_{T=\bar{T}} + \frac{\partial C}{\partial T}\bigg|_{\substack{T=\bar{T} \\ \dot{m}=\bar{m}}} \right) \bar{T} - \frac{\partial C}{\partial \dot{m}}\bigg|_{\substack{T=\bar{T} \\ \dot{m}=\bar{m}}} \bar{m} + \begin{bmatrix} \frac{Pk}{\rho c_p A} T_\infty \\ \frac{Pk}{\rho c_p A} T_\infty \\ \frac{Pk}{\rho c_p A} T_\infty \end{bmatrix} + D\psi(T,t) \tag{4.54}$$

which would give matrix A as

$$\begin{bmatrix} A_{11} + \left(\frac{\partial B_1}{\partial T_1} + \frac{\partial C_1}{\partial T_1}\right)\Big|_{T=\bar{T}} & A_{12} + \left(\frac{\partial B_1}{\partial T_2} + \frac{\partial C_1}{\partial T_2}\right)\Big|_{T=\bar{T}} & A_{13} + \left(\frac{\partial B_1}{\partial T_3} + \frac{\partial C_1}{\partial T_3}\right)\Big|_{T=\bar{T}} \\ A_{21} + \left(\frac{\partial B_2}{\partial T_1} + \frac{\partial C_2}{\partial T_1}\right)\Big|_{T=\bar{T}} & A_{22} + \left(\frac{\partial B_2}{\partial T_2} + \frac{\partial C_2}{\partial T_2}\right)\Big|_{T=\bar{T}} & A_{23} + \left(\frac{\partial B_2}{\partial T_3} + \frac{\partial C_2}{\partial T_3}\right)\Big|_{T=\bar{T}} \\ A_{31} + \left(\frac{\partial B_3}{\partial T_1} + \frac{\partial C_3}{\partial T_1}\right)\Big|_{T=\bar{T}} & A_{32} + \left(\frac{\partial B_3}{\partial T_2} + \frac{\partial C_3}{\partial T_2}\right)\Big|_{T=\bar{T}} & A_{33} + \left(\frac{\partial B_3}{\partial T_3} + \frac{\partial C_3}{\partial T_3}\right)\Big|_{T=\bar{T}} \end{bmatrix} \begin{bmatrix} T_1 \\ T_2 \\ T_3 \end{bmatrix} \tag{4.55}$$

where

$$\begin{aligned} \frac{\partial B_1}{\partial T_1} &= -\frac{e^{10(T_2-T_1}}{2(1+e^{10(T_2-T_1))}}, \quad \frac{\partial B_1}{\partial T_2} = \frac{e^{10(T_2-T_1}}{2(1+e^{10(T_2-T_1))}}, \quad \frac{\partial B_1}{\partial T_3} = 0 \\ \frac{\partial B_2}{\partial T_1} &= \frac{e^{10(T_2-T_1)}}{2(1+e^{10(T_2-T_1))}}, \quad \frac{\partial B_2}{\partial T_2} = -\frac{e^{10(T_3-T_2)}}{2(1+e^{10(T_3-T_2))}} + \frac{e^{10(T_2-T_1)}}{2(1+e^{10(T_2-T_1)})} \\ \frac{\partial B_2}{\partial T_3} &= \frac{e^{10(T_3-T_2)}}{2(1+e^{10(T_3-T_2))}}, \quad \frac{\partial B_3}{\partial T_1} = 0, \quad \frac{\partial B_3}{\partial T_2} = \frac{e^{10(T_3-T_2)}}{2(1+e^{10(T_3-T_2))}}, \\ \frac{\partial B_3}{\partial T_3} &= -\frac{e^{10(T_3-T_2)}}{2(1+e^{10(T_3-T_2))}} \quad \text{and} \quad \Big|_{T=\bar{T}} \quad \forall \quad \frac{\partial B_i}{\partial T_i} \end{aligned} \tag{4.56}$$

The partial derivatives of C_i with respect to T_i are too large and complex to put completely and clearly in a matrix, so that will be done only in the simulating part of the model in MATLAB. The partial derivatives of C_i with respect to $\dot{m}$ can be seen easily, as $\dot{m}$ is the same for each layer. The partial derivative will result in the formulas of 2.12, 2.13, 2.14, 2.15, 2.16 and 2.17, where the $\dot{m}$ will replaced with $1 \ \forall \ \frac{\partial C_i}{\partial \dot{m}}$. Now the system has been linearized, the most important feature that needs to be checked, is whether the definition of matrix D, will still allow the design of G_n, or if that is not possible, whether the error formula $(A_{11} + LA_{21})e(t)$ is asymptotically stable. The formula for D looks like

$$D = G_n X = \begin{bmatrix} L \\ -I_p \end{bmatrix} X \tag{4.57}$$

for some random, to be designed $X \in \mathbb{R}^{2\times 2}$. Where D is known, so it is possible to check whether the design matrix G_n can exist. First of all, the matrix D needs to be transformed into the new coordination system multiplying T_c(4.3) with D:

$$\begin{bmatrix} 0 & 1 & 0 \\ 1 & 0 & 0 \\ 0 & 0 & 1 \end{bmatrix} * \begin{bmatrix} 1 & 0 \\ -1 & -1 \\ 0 & 1 \end{bmatrix} = \begin{bmatrix} -1 & 1 \\ 1 & 0 \\ 0 & -1 \end{bmatrix} \tag{4.58}$$

Now the general formula of G_nX can be calculated to check whether it is possible to reach the form of the transformed matrix D.

$$G_nX = \begin{bmatrix} L \\ -I_p \end{bmatrix} X = \begin{bmatrix} L_1 & L_2 \\ -1 & 0 \\ 0 & -1 \end{bmatrix} * \begin{bmatrix} x_1 & x_2 \\ x_3 & x_4 \end{bmatrix} \tag{4.59}$$

$$= \begin{bmatrix} L_1x_1 + L_2x_3 & L_1x_2 + L_2x_4 \\ -x_1 & -x_2 \\ -x_3 & -x_4 \end{bmatrix} \tag{4.60}$$

which must be equal to the transformed matrix D (4.58). It shows that there are two zeros on places [2,2] and [3,1] in matrix D. This means that x_2 and x_3 must equal zero. Resulting in:

$$\begin{bmatrix} L_1x_1 & L_2x_4 \\ -x_1 & 0 \\ 0 & -x_4 \end{bmatrix} \tag{4.61}$$

where entry [2,1] must be 1 and entry [3,2] must be -1, giving $x_1 = -1$ and $x_4 = 1$. Resulting in values of 1 for both L_1 and L_2. This would correctly give

$$\begin{bmatrix} L_1x_1 & L_2x_4 \\ -x_1 & 0 \\ 0 & -x_4 \end{bmatrix} = \begin{bmatrix} 1*-1 & 1*1 \\ -(-1) & 0 \\ 0 & -(1) \end{bmatrix} = \begin{bmatrix} -1 & 1 \\ 1 & 0 \\ 0 & -1 \end{bmatrix} \tag{4.62}$$

showing that it is possible to design L and X such that it complies with the constraint 4.57. However, it shows that the total design freedom from the observer gain L is now eliminated, as L_1 and L_2 must now equal 1 for the constraint and thereby, the observer to hold. Since the design freedom for L is now zero, the most important aspect is to check whether this holds

$$\dot{e_1}(t) = (A_{11} + LA_{22})e(t) < 0 \tag{4.63}$$

meaning that the error is asymptotically stable. This can be explored by transforming matrix A and looking at the value of the error. This is shown as

$$T_cAT_C^{-1} = \begin{bmatrix} 0 & 1 & 0 \\ 1 & 0 & 0 \\ 0 & 0 & 1 \end{bmatrix} \begin{bmatrix} -\frac{a}{z^2} - \frac{Pk}{\rho c_p A} & \frac{a}{z^2} & 0 \\ \frac{a}{z^2} & -2\frac{a}{z^2} - \frac{Pk}{\rho c_p A} & \frac{a}{z^2} \\ 0 & \frac{a}{z^2} & -\frac{a}{z^2} - \frac{Pk}{\rho c_p A} \end{bmatrix} \begin{bmatrix} 0 & 1 & 0 \\ 1 & 0 & 0 \\ 0 & 0 & 1 \end{bmatrix} \tag{4.64}$$

$$= \begin{bmatrix} -2\frac{a}{z^2} - \frac{Pk}{\rho c_p A} & \frac{a}{z^2} & \frac{a}{z^2} \\ \frac{a}{z^2} & -\frac{a}{z^2} - \frac{Pk}{\rho c_p A} & 0 \\ \frac{a}{z^2} & 0 & -\frac{a}{z^2} - \frac{Pk}{\rho c_p A} \end{bmatrix} \tag{4.65}$$

where it can be seen that

$$A_{11} = -2\frac{a}{z^2} - \frac{Pk}{\rho c_p A} \quad and \quad A_{21} = \begin{bmatrix} \frac{a}{z^2} \\ \frac{a}{z^2} \end{bmatrix} \tag{4.66}$$

resulting in the error function

$$\dot{e_1}(t) = (A_{11} + LA_{22})e(t) \tag{4.67}$$

$$= \left(-2\frac{a}{z^2} - \frac{Pk}{\rho c_p A} + \begin{bmatrix} 1 & 1 \end{bmatrix} \begin{bmatrix} \frac{a}{z^2} \\ \frac{a}{z^2} \end{bmatrix} \right) e(t) \tag{4.68}$$

$$= \left(-2\frac{a}{z^2} - \frac{Pk}{\rho c_p A} + 2\frac{a}{z^2} \right) e(t) \tag{4.69}$$

$$= -\frac{Pk}{\rho c_p A} e(t) \tag{4.70}$$

which is strictly negative, because each individual parameter must be positive. This shows, that for the current model with three layers it is possible to observer the middle state as the error will converge to zero. The model can now be simulated in MATLAB and Simulink by implementing both the mathematical system as the observer. The simulations and results will be discussed in the next chapter.

5 Simulations and Results

A number of simulations were performed in MATLAB and Simulink. The values for some parameters need to be determined. The ρ, c_p, and α have already been established in Chapter 3 and Appendix B. So the parameters that need to be established are P, k, A, z and T_∞. The area, perimeter and height per layer can be deducted from the capacity of the tank. In this research, we will consider a tank of 1000 m^3 with a height of 15 m. This can give z=5m, A=66,7m, and P=13,7m. Since most thermal storage tanks are placed underground, it is realistic to take the soil temperature for T_∞ which is 11 $°C$ average in the Netherlands according to [10]. The thermal conductivity of isolation walls usually is between 0,02-0,04 $W/m°C$ ([KIs]), so an average of 0,03 $W/m°C$ is taken. If the tank were to be charged in 4 hours, the $\dot{m}$ should be approximately 68 kg/s for initial temperatures of T_1=25 $°C$, T_2=20 and T_3=15 $°C$ assuming that0 80 $°C$ represents a full charge. Furthermore, the discharge temperature will be 50 $°C$. The complete Simulink layout and the MATLAB code can be found in Appendix C.

For the normal values, the observer does converge to zero without disturbances. However, it takes incredibly long. This happens because the error function is negative but minuscule, as shown by

$$-\left(\frac{Pk}{\rho c_p A}\right)e(t) = -\frac{13,7 * 0,03}{988,04 * 4026 * 66,7}e(t) = -1,55 * 10^{-9}e(t) \tag{5.1}$$

which shows that the observer cannot be used for commercial or applicable academic purposes, as the error will never converge to zero quickly. It will take approximately a month for the error to reduce by 0,5 $°C$. However, it is still possible to check whether the observer would work for fictional numbers for a contribution to the academic field.

Defining the inflow and outflow to be zero, β=100 and all other parameter to be equal to 1. The initial temperature conditions are T1=80$°C$, T2=70$°C$, and T3=60$°C$, and the initial values for $\hat{T}$ are 0,9T_i. The linearization is taken at $\bar{T}1 = 40°C$, $\bar{T}2 = 30°C$ and $\bar{T}3 = 20°C$. These values are chosen due to the behavior of the normal system; when $\dot{m} = 1$ is applied, the normal system reaches exactly these values of T during charging, showing that these are proper values for $\bar{T}$. This gives a convergence of the error in a couple of seconds, shown in figure 4. Here, layer 2 needs to be reconstructed by the observer, and it shows that the reaching mode takes approximately 1/10th of a second, and then it reaches the sliding mode, where the error of the state converges to zero in approximately 5 seconds. The total simulation time is 10 seconds. Figure 4 shows that the Sliding Mode Observer does work very well for fictional parameters with no charging or perturbations.

Now, a simulation with charging and discharging of the tank can be considered to see whether this will give accurate results as well. All the conditions will remain the same, except for the $\dot{m}_1$ and $T_{supply} = 80°C$. There will be charging of the tank between t=20 and t=40, with $\dot{m}_1 = 1kg/s$. This will result in figure 5. The figure depicts that the error dynamics, until the charging starts, look the same as in figure 4. However, at t=20, when the charging starts, it can be seen that an error occurs, and the observer moves into the reaching mode for shorter than a second and then reaches the sliding mode. The sliding mode takes approximately 3 seconds before the error converges to zero. The total simulation time is 40 seconds. This figure shows that the observer also works for fictional parameters during charging without disturbance.

The subsequent simulations include the error dynamics, D$\omega(T, y)$, in the simulations. This will check whether the Sliding Mode Observer works with perturbations in the system. All the other parameters remain the same, just as the $\dot{m}_1$. The results are shown in figure 6. The plot shows that the error dynamics remain almost the same, as no changes can be seen without zooming. The total simulation time is 40 seconds. This shows that the sliding mode observer can indeed reconstruct the unknown state (T2) while the system has parameter uncertainty and measurement noise for these parameters and charging circumstances.

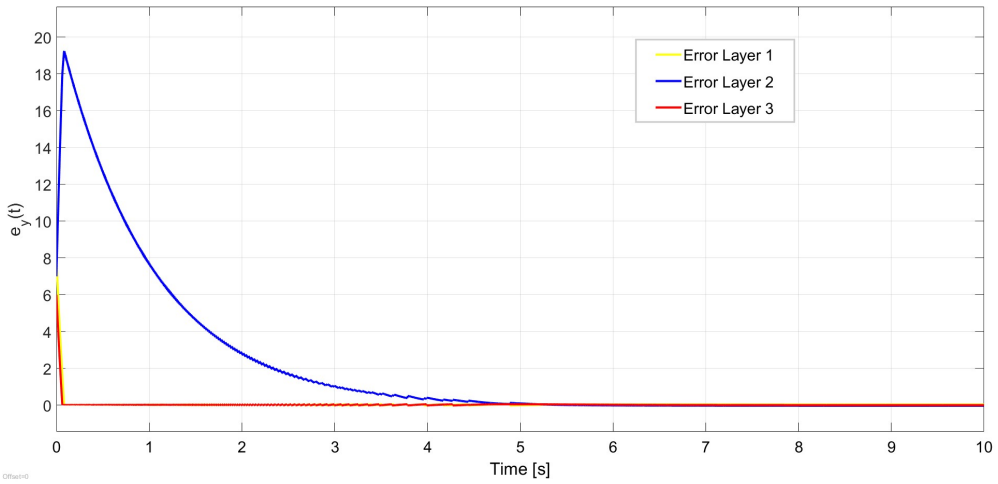

Figure 4: *Observer error without disturbance or flow*

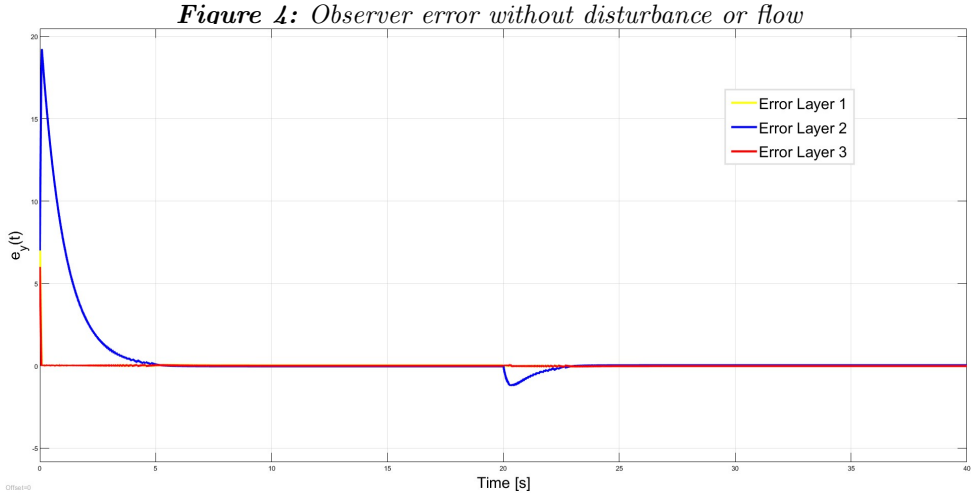

Figure 5: *Observer error with charging between* $20 \leq t \leq 40$

Now that these results are shown, it is important to check whether adding a discharging phase is possible. This can be added after the charging phase. The following conditions are added: $\dot{m} = 0$ for $0 < t < 20 \wedge 30 < t \leq 40 \wedge t > 50$, $\dot{m} = 1$ for $20 \leq t \leq 30$ and $\dot{m} = -1$ for $40 \leq t \leq 50$, where $T_{discharge} = 50°C$. The total simulation time is 70 seconds. Figure 7 shows that that the error dynamics behave just like the previous plots until 30 seconds. However, a negative error forms when the charging stops at 30 seconds. When the discharging starts at 40 seconds, the error increases, and after the discharging has stopped, an even bigger negative error forms. This could happen due to two things, firstly since the linearization values for $\bar{T}$, that is still at $\bar{T}1 = 40°C$, $\bar{T}2 = 30°C$ and $\bar{T}3 = 20°C$ only work for a close region of T to the linearization values. The linearization could causes problems for the observer, when there are charging and discharging periods in the same simulation, because the values for $\bar{T}$ are only appropriate around the region the values are chosen and since the T_{charge} and $T_{discharge}$ have different outcomes for the real system, it might be possible that the error will not converge because of this. The second possibility is that the discharging temperature $T_{discharging} = 50°C$, is hotter than the temperature in the tank. This causes problems for the observer.

In figure 8, the linearization values for $\bar{T}$ have been lowered to 11 $°C$ for each $\bar{T}$. All other parameters

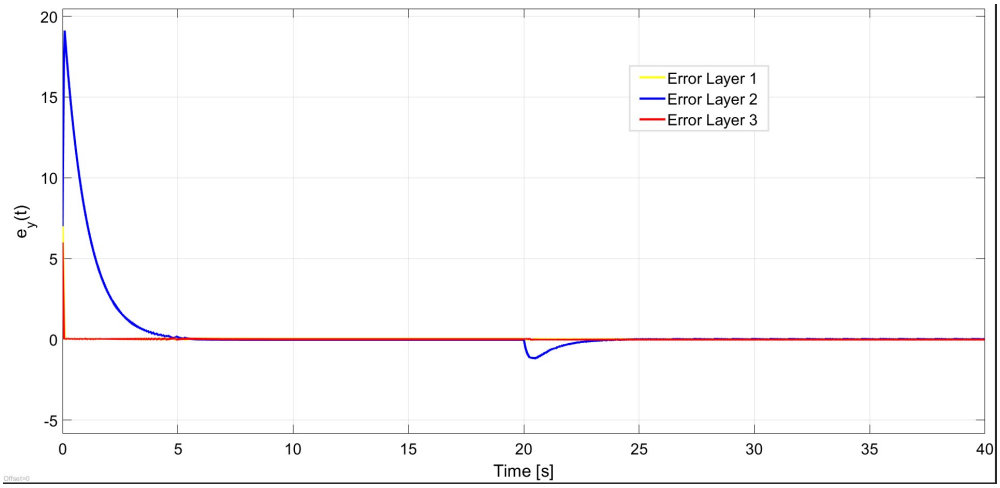

Figure 6: *Observer error with charging between* $20 < t < 40$ *and added error dynamics* $D\omega$

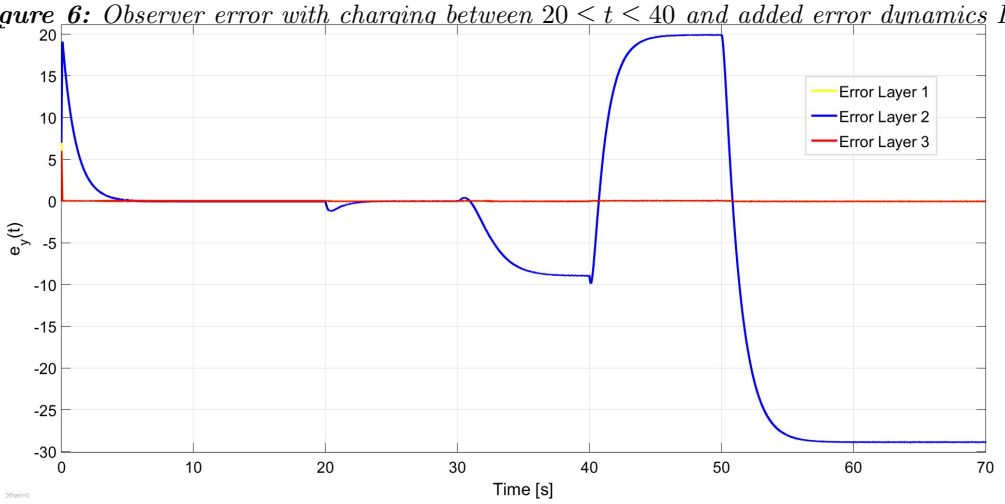

Figure 7: *Observer error with charging between* $20 \leq t \leq 30$ *and discharging between* $40 \leq t \leq 50$ *and added error dynamics* $D\omega$

remain the same, just like the charging and discharging between 20 and 30 seconds and 40 and 50 seconds respectively. This figure 8 shows that there is still an error during the discharging. However, after the discharging ends, it will converge back to zero. Setting the linearization values at T_∞ allows this. In figure 9, all the parameters have the same values as in figure 7, only the $T_{discharge}$ is lowered to $5°C$. This figure shows that the error does not converge but remains negative after the discharging stops. Figures 8 and 9 do not exactly show what the cause is. However, it does show that the values for $\bar{T}$ are important for the convergence after the discharging stops.

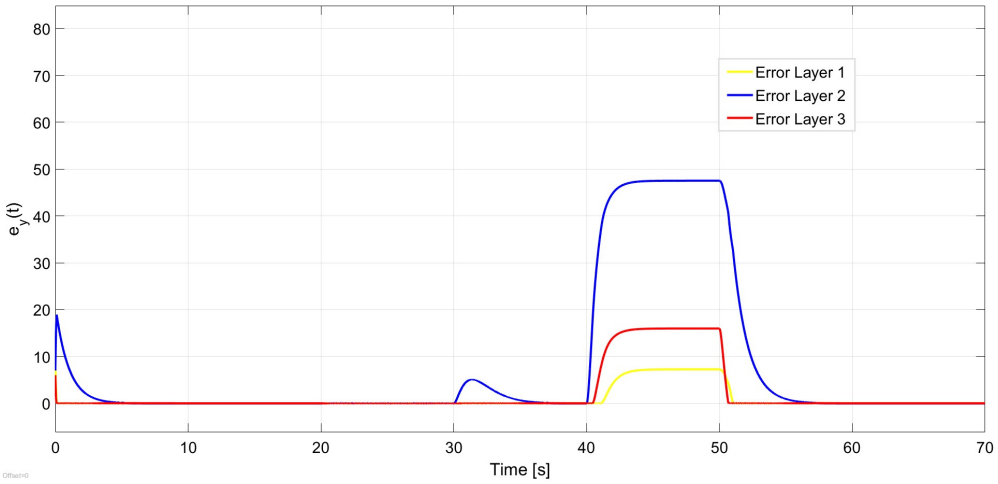

Figure 8: *Observer error with charging between* $20 \leq t \leq 30$*, discharging between* $40 \leq t \leq 50$*, added error dynamics* $D\omega$ *and* $\bar{T} = 11°C$

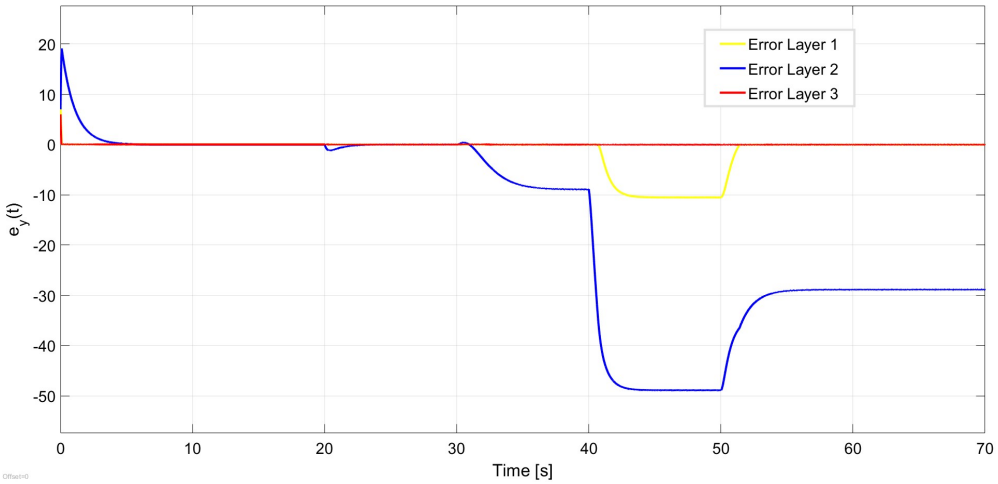

Figure 9: *Observer error with charging between* $20 \leq t \leq 30$*, discharging between* $40 \leq t \leq 50$*, added error dynamics* $D\omega$ *and* $T_{discharge} = 5°C$

6 Conclusion

In this research, a 1-dimensional mathematical model for a stratified thermal storage tank is derived from literature. This model is discretized through space to transform it into an ODE. Furthermore, the effects of slow buoyancy and mixing are explained thoroughly and are added to the basic mathematical model. The final mathematical model is detailed enough and explained well enough to be used for observation methods such as the Sliding Mode. For this model, multiple different designs of Sliding Mode Observers are reviewed to check whether they would fit the model and get results. First, a linear sliding mode observer without disturbances is explained in small steps to give a broader proficiency on how the sliding mode generally operates. It was verified that under model linearization it can be implemented into the system model. Secondly, a sliding mode observer with disturbances is explained, which cannot be applied to the model since the disturbance matrix did not satisfy a fundamental matching condition needed for the implementation of the observer. Thirdly, a sliding mode observer for a nonlinear system with disturbances is briefly discussed, and the model did also not met the matching condition. This shows that it is impossible to use a Sliding Mode based observer design as discussed in chapter 3 in the book from [30], when we consider at once all the disturbances that our model can be subjected to. There is a change possible in the disturbance and the matrix D for the disturbance, to enable the design of an observer for both a linear as a nonlinear system. This would not include the complete disturbance, so it is not applicable to real-life applications. However, the simulations of that linear observer with disturbances show that the error converges, even though it takes years, which is too long for any commercial or academic purpose. It takes so long to converge, because the design freedom of the observer gain is eliminated by the altered design of the disturbance matrix. When applying fictional numbers to the observer to increase the convergence time, the error does converge in a very short time. It also converges with perturbations and while charging. However, when adding a discharging phase, the simulations show that the error does not converge during the discharging, only after discharging stops. The proof that it is impossible to design an adequate Sliding Mode Observer for the complete mathematical model using the observer design from the book [30] answers the research question.

7 Discussion

This research focused on reviewing the possibilities for an observer design using the sliding mode control technique. First, the mathematical model was deducted and included and thoroughly explained the terms for slow buoyancy and mixing. This mathematical model can be used in future research. Secondly, the bounded disturbance function that is required for a Sliding Mode Observer Design and other kinds of state estimation strategies has been entirely derived from literature. This disturbance function can be used in further research within the sliding mode, or for other types of SES that need a bounded disturbance function; besides this, the parameter error or measurement noise for a parameter can individually be used in future research as well. Then, the first possible sliding mode observer is reviewed. This is for a linear system without disturbance, and the thorough explanation shows that this applies to the derived mathematical model. Future research could empirically analyze whether such an observer would work if it were to be applied to a real stratified thermal storage tank. A Sliding Mode Observer for a linear system with disturbances needs total design freedom for the disturbance matrix. This research contributes to the academic field by proving that such an observer cannot be designed for the 1-dimensional mathematical model. Lastly, a sliding mode observer for a nonlinear system with perturbations is reviewed. This research contributes to the scientific field by proving that the mathematical model cannot comply with this observer's constraints. The non-cooperating constraints can be avoided by designing smaller and less complete disturbance dynamics with corresponding matrix. By doing this, an observer can be designed. The limitations of this design are the linearization of the mathematical model and the evaluation of $\bar{T}$. This research proves that the observer converges for the correct evaluation values of $\bar{T}$ with an disturbance and during constant charging.

Further research could look into designing a nonlinear sliding mode observer for the smaller disturbance dynamics and corresponding matrix. Future research could also look into more modern sliding mode observers with different designs, as there are other possible designs using the sliding mode technique. In this research, there are several working assumptions and simplifications. Such that the model only has three layers, and the volume remains constant. If a sufficient sliding mode observer were to be designed, these working assumptions should be examined to see whether they significantly impact the observer's dynamics. Besides this, the mathematical model is 1-dimensional, while a real stratified thermal storage tank can only be described entirely by a 3-dimensional model. For optimization methods, a 1-dimensional model often satisfies. However, for further research, it could be possible to look at a more complicated model, which could possibly avoid the constraints for a sliding mode observer design. The computational time could be an issue for a 3-dimensional mode and should be considered wisely. Another point of further research could be to look into the design of the disturbance function. The changes made to reduce and simplify the disturbance dynamics and corresponding matrix in this research do not suffice for real-life applications. Further research could look into the design of the bounded disturbance function and ways to avoid the constraint of the size of the disturbance matrix. Lastly, reviewing other state estimation strategies is also something to consider for estimating the temperature profile of a stratified thermal storage tank in future research.

References

[KIs] Insulation materials and their thermal properties. https://www.greenspec.co.uk/building-design/insulation-materials-thermal-properties/. Accessed: 26-01-2023.

[2] Water - density, specific weight and thermal expansion coefficients. https://www.engineeringtoolbox.com/water-density-specific-weight-d_595.html. Accessed: 08-01-2023.

[3] Water - specific heat vs. temperature. https://www.engineeringtoolbox.com/specific-heat-capacity-water-d_660.html. Accessed: 08-01-2023.

[4] Water - thermal diffusivity vs. temperature and pressure. https://www.engineeringtoolbox.com/water-steam-thermal-diffusivity-d_2058.html. Accessed: 08-01-2023.

[5] Chandra, Y. P. and Matuska, T. (2019). Stratification analysis of domestic hot water storage tanks: A comprehensive review. *Energy and Buildings*, 187:110–131.

[6] Childs, P. R., Greenwood, J., and Long, C. (2000). Review of temperature measurement. *Review of scientific instruments*, 71(8):2959–2978.

[7] De Ridder, F. and Coomans, M. (2014). Grey-box model and identification procedure for domestic thermal storage vessels. *Applied thermal engineering*, 67(1-2):147–158.

[8] Guelpa, E. and Verda, V. (2019). Thermal energy storage in district heating and cooling systems: A review. *Applied Energy*, 252:113474.

[9] Hastie, T., Tibshirani, R., and Friedman, J. (2001). The elements of statistical learning. springer series in statistics. *New York, NY, USA*.

[10] Jacobs, A. F., Heusinkveld, B. G., and Holtslag, A. A. (2011). Long-term record and analysis of soil temperatures and soil heat fluxes in a grassland area, the netherlands. *Agricultural and Forest Meteorology*, 151(7):774–780.

[11] Joelsson, A. and Gustavsson, L. (2009). District heating and energy efficiency in detached houses of differing size and construction. *Applied Energy*, 86(2):126–134.

[12] Kashima, A., Lee, P. J., Ghidaoui, M. S., and Davidson, M. (2013). Experimental verification of the kinetic differential pressure method for flow measurements. *Journal of hydraulic research*, 51(6):634–644.

[13] Kashima, A., Lee, P. J., and Nokes, R. (2012). Numerical errors in discharge measurements using the kdp method. *Journal of hydraulic research*, 50(1):98–104.

[14] Khalil, H. K. (2002). *Nonlinear Systems*. Prentice Hall.

[15] Kobari, T., Okajima, J., Komiya, A., and Maruyama, S. (2015). Development of guarded hot plate apparatus utilizing peltier module for precise thermal conductivity measurement of insulation materials. *International Journal of Heat and Mass Transfer*, 91:1157–1166.

[16] Kreuzinger, T., Bitzer, M., and Marquardt, W. (2008). State estimation of a stratified storage tank. *Control Engineering Practice*, 16(3):308–320.

[17] Lago, J., De Ridder, F., Mazairac, W., and De Schutter, B. (2019). A 1-dimensional continuous and smooth model for thermally stratified storage tanks including mixing and buoyancy. *Applied Energy*, 248:640–655.

[18] Lund, H., Østergaard, P. A., Chang, M., Werner, S., Svendsen, S., Sorknæs, P., Thorsen, J. E., Hvelplund, F., Mortensen, B. O. G., Mathiesen, B. V., et al. (2018). The status of 4th generation district heating: Research and results. *Energy*, 164:147–159.

[19] Marx, W., Haunschild, R., and Bornmann, L. (2021). Heat waves: a hot topic in climate change research. *Theoretical and applied climatology*, 146(1-2):781–800.

[20] Mazhar, A. R., Liu, S., and Shukla, A. (2018). A state of art review on the district heating systems. *Renewable and Sustainable Energy Reviews*, 96:420–439.

[21] Min, S.-K., Zhang, X., Zwiers, F. W., and Hegerl, G. C. (2011). Human contribution to more-intense precipitation extremes. *Nature*, 470(7334):378–381.

[22] Morales Sandoval, D. A., De La Cruz Loredo, I., Bastida, H., Badman, J. J., and Ugalde-Loo, C. E. (2021). Design and verification of an effective state-of-charge estimator for thermal energy storage. *IET Smart Grid*, 4(2):202–214.

[23] Njoku, H., Ekechukwu, O., and Onyegegbu, S. (2014). Analysis of stratified thermal storage systems: An overview. *Heat and mass transfer*, 50(7):1017–1030.

[24] Oliveski, R. D. C., Krenzinger, A., and Vielmo, H. A. (2003). Comparison between models for the simulation of hot water storage tanks. *Solar Energy*, 75(2):121–134.

[25] O'neill, M. (1966). Measurement of specific heat functions by differential scanning calorimetry. *Analytical chemistry*, 38(10):1331–1336.

[26] Perruquetti, W. and Barbot, J. P. (2002). *4.1 Sliding Mode Observers: Introduction*, page 119–120. Dekker.

[27] Rudtsch, S. (2002). Uncertainty of heat capacity measurements with differential scanning calorimeters. *Thermochimica acta*, 382(1-2):17–25.

[28] Salmon, D. (2001). Thermal conductivity of insulations using guarded hot plates, including recent developments and sources of reference materials. *Measurement Science and Technology*, 12(12):R89.

[29] Samantaray, J. and Chakrabarty, S. (2020). Discrete time sliding mode control. In Volosencu, C., Saghafinia, A., Du, X., and Chakrabarty, S., editors, *Control Theory in Engineering*, chapter 5. IntechOpen, Rijeka.

[30] Shtessel, Y., Edwards, C., Fridman, L., and Levant, A. (2015). *3 Conventional Sliding Mode Observers*, page 105–136. Birkhauser.

[31] Smith, G. D., Smith, G. D., and Smith, G. D. S. (1985). *Numerical solution of partial differential equations: finite difference methods*. Oxford university press.

[32] Soares, A., Camargo, J., Al-Koussa, J., Diriken, J., Van Bael, J., and Lago, J. (2022). Efficient temperature estimation for thermally stratified storage tanks with buoyancy and mixing effects. *Journal of Energy Storage*, 50:104488.

[33] Tanaka, M., Girard, G., Davis, R., Peuto, A., and Bignell, N. (2001). Recommended table for the density of water between 0 c and 40 c based on recent experimental reports. *Metrologia*, 38(4):301.

[34] Zhang, H., Shang, C., and Tang, G. (2022). Measurement and identification of temperature-dependent thermal conductivity for thermal insulation materials under large temperature difference. *International Journal of Thermal Sciences*, 171:107261.

[35] Zhang, Y. and Srivastava, A. (2009). Accurate temperature estimation using noisy thermal sensors. In *2009 46th ACM/IEEE Design Automation Conference*, pages 472–477. IEEE.

A Tables

Temperature in $°C$	**Density in** kg/m^3	**Deviation in** %	**Absolute Deviation in** kg/m^3
0,1	999,85	1,18	11,81
10	999,7	1,17	11,66
15	999,1	1,11	11,06
20	998,21	1,02	10,17
25	997,05	0,90	9,01
30	995,65	0,76	7,61
35	994,03	0,60	5,99
40	992,22	0,42	4,18
45	990,21	0,22	2,17
50	988,04	0,00	0
55	985,69	0,24	2,35
60	983,2	0,49	4,84
65	980,55	0,76	7,49
70	977,76	1,05	10,28
75	974,84	1,35	13,2
80	971,79	1,67	16,25
85	968,61	2,01	19,43
90	965,31	2,35	22,73
95	961,89	2,72	26,15
100	958,35	3,10	29,69

Table 1: *Deviation for temperature differences when* ρ *is constant at* $\rho = 988,04 kg/m^3$

Temperature in $°C$	**Specific Heat Capacity in** $kJ/kg * T$	**Deviation in** %	**Absolute Deviation in** $kJ/kg * T$
0,01	4,217	4,53	0,191
10	4,191	3,93	0,165
20	4,157	3,14	0,131
30	4,118	2,21	0,091
40	4,074	1,16	0,047
50	4,026	0,00	0,000
60	3,977	1,25	0,050
70	3,925	2,58	0,101
80	3,873	3,96	0,153
90	3,820	5,39	0,206
100	3,768	6,85	0,258

Table 2: *Deviation for temperature differences when* c_p *is constant at* $c_p = 4,026$

Temperature in $°C$	**Fluid Diffusivity in** $10^{-6}\ m^2/s$	**Deviation in** $\%$	**Absolute Deviation in** $10^{-6}\ m^2/s$
0	0,132	17,42	0,023
5	0,135	14,81	0,02
10	0,138	12,32	0,017
20	0,143	8,39	0,012
25	0,146	5,81	0,009
30	0,148	4,52	0,007
50	0,155	0,00	0
75	0,162	4,32	0,007
100	0,168	7,74	0,013

Table 3: *Deviation for temperature differences when* α *is constant at* $\alpha = 0,155$

B Lyapunov Stability

Consider the following autonomous system

$$\dot{x}(t) = f(t, x) \quad x \in \mathbb{R}^n \tag{B.1}$$

An equilibrium point for the equation is given as

$$f(x_0, t) = 0 \ \forall \ t > 0 \tag{B.2}$$

there may be much more x_0 that satisfy this condition. However, for analyzing stability properties, it is useful to assume that the equilibrium lies at the origin $x \in \mathbb{R}^n$. There is no loss of generality, since any equilibrium point can be shifted to the origin through a change of variable $x \to \bar{x}$ where $\bar{x} = x - x_0$ implies the origin is an equilibrium point of

$$\dot{\bar{x}}(t) = f(t, \bar{x}) \quad \bar{x} \in \mathbb{R}^n, \quad \text{so} \quad f(x_0, t) = 0 = f(t, \bar{x} = 0) \tag{B.3}$$

showing that the assumption for a equilibrium point in the origin does not result in loss of generality.

Definition 1. The equilibrium point of B.2, x=0 is stable if for each $\epsilon > 0$, there is a $\delta = \delta(\epsilon) > 0$, such that

$$\text{for} ||x(0)|| < \delta \text{there is} ||x(t)|| < \epsilon, \ \forall \ t \geq 0 \tag{B.4}$$

Meaning that starting close enough to the equilibrium point, the solution will always remain close to it. The solution is unstable if it is not stable and it is asymptotically stable if it is stable and δ can be chosen such that

$$\text{for} ||x(0)|| < \delta \text{there is} \lim_{t \to \infty} x(t) = 0 \tag{B.5}$$

Meaning that by starting close to the equilibrium point, it will always remain close and in addition, it will move towards the equilibrium point.

Theorem 1. Let x=0 be an equilibrium point for B.1 and let $D \subset \mathbf{R}^n$ be a domain containing x=0. Let $V : D \to R$ be an ODE such that

$$V(0) = 0 \quad \text{and} \quad V(x) > 0 \quad \text{in} \quad D \backslash \{0\} \tag{B.6}$$

where

$$\dot{V}(x) = \frac{\partial V}{\partial t} + \frac{\partial V}{\partial x} f(t, x) \leq 0 \quad \text{in} \quad D \tag{B.7}$$

then x=0 is stable. Furthermore, if

$$\dot{V}(x) < 0 \quad \text{in} \quad D \tag{B.8}$$

then x=0 is asymptotically stable. As this only contains a domain D in all real numbers, this does not prove global asymptotic stability. There are two more constraints for global asymptotic stability. The first one is very intuitive, namely the conditions of Theorem 1 must hold for D = $\mathbb{R}^n$. The other constraint that must hold is

$$||x|| \to \infty \implies V(x) \to \infty \tag{B.9}$$

If a function V complies to these constraints, it is called a radially unbounded funnction.
Theorem 2. Conside the system B.1. If this function is radially unbounded, positive definite and differentiable $V : \mathbb{R} \times \mathbb{R}^n \to \mathbb{R}$

$$\dot{V}(x) = \frac{\partial V}{\partial t} + \frac{\partial V}{\partial x} f(t, x) \leq 0 \quad \text{in} \quad D \tag{B.10}$$

then the is global stable. Furthermore, if

$$\dot{V}(x) < 0 \quad \text{for} \quad x \neq 0 \tag{B.11}$$

then the origin is asymptotically stable. This appendix uses both the appendix D of [30] and chapter 4.1 from [14] to explain the Lyapunov Stability for local and global situations.

C Matlab and Simulink Model

This appendix shows the MATLAB model in which the parameters and initial values are defined, and where the linearization is performed. Furthermore it contains the Simulink file with the content of each block.

The MATLAB data:

```
1
2  clear all
3
4
5  %%% Numerical values of some parameters
6  alpha=1;
7  rho=1;
8  A=1;
9  dz=1;
10 cp=1;
11 P=1;
12 k=1;
13 Beta=100;
14
15 %%% Values of the ambient temperature, charging temperature and the
16 %%% discharging temperature
17 T_amb=11;
18 T_sup=80;
19 T_ret=5;
20 K_mdot=5;
21
22
23 %%% Specification of the initial conditions
24 T0=[80;70;60];
25 T_hat0=0.9*T0;
26 mdot_0=0;
27
28 %%% Linearization of lambda, by defining the jacobian matrix
29
30 %%% Defining the values of T and T_hat as real, so they can be used
       in the
31 %%% linearization
32 syms T1 real
33 syms T2 real
34 syms T3 real
35
36 syms T_hat1 real
37 syms T_hat2 real
38 syms T_hat3 real
39
40 syms mdot real
41
42
43 %%% The values for which the Temperature will be evaluated, this is
       \bar{T}
44 %%% in the report
```

```
T1nom=11;
T2nom=11;
T3nom=11;

%%% The values for which the mass flow will be evaluated, this is \bar{\dot{m}}
%%% in the report
mdotnom=1;


%%%Linearzing Lambda
LAMBDA=@(T1,T2,T3)[(1/20)*log(1+exp(10*(T2-T1)));
    -(1/20)*log(1+exp(10*(T2-T1)))+(1/20)*log(1+exp(10*(T3-T2)));
    -(1/20)*log(1+exp(10*(T3-T2)))];


JAC_LAMBDA=jacobian(LAMBDA(T1,T2,T3),[T1,T2,T3]);

JAC_LAMBDA_EVAL=matlabFunction(JAC_LAMBDA);

%%% Defining the output of Lambda, so it can be used in the Simulink block
%%% for the observer
lambda_nom=LAMBDA(T1nom,T2nom,T3nom);
jac_lambda_nom=JAC_LAMBDA_EVAL(T1nom,T2nom,T3nom);


%%%Linearzing the convection for the charging
CONV_CHARGING=@(T1,T2,T3,mdot)[(1/(dz*rho*A))*(mdot*(T_sup-T1));
    (1/(dz*rho*A))*(mdot*(T1-T2));
    (1/(dz*rho*A))*(mdot*(T2-T3))];

%%%Defining and evaluating the Jacobian Matrix with respect to T for charging
JAC_CONV_T_CHARGING=jacobian(CONV_CHARGING(T1,T2,T3,mdot),[T1,T2,T3]);

JAC_CONV_T_EVAL_CHARGING=matlabFunction(JAC_CONV_T_CHARGING);

%%%Defining and evaluating the Jacobian Matrix with respect to Mdot for charging
JAC_CONV_mdot_CHARGING=jacobian(CONV_CHARGING(T1,T2,T3,mdot),mdot);

JAC_CONV_mdot_EVAL_CHARGING=matlabFunction(JAC_CONV_mdot_CHARGING);

%%% Defining the values for the Jacobian for the charging, so it can be implemented in the
%%% observer
conv_nom=CONV_CHARGING(T1nom,T2nom,T3nom,mdotnom);

jac_conv_T=JAC_CONV_T_EVAL_CHARGING(mdotnom);
```

```
90
91  jac_conv_mdot=JAC_CONV_mdot_EVAL_CHARGING(T1nom,T2nom,T3nom);
92
93
94  %%%Linearzing the convection for the discharging
95  CONV_DISCHARGING=@(T1,T2,T3,mdot)[(1/(dz*rho*A))*(mdot)*(T2-T1);
96      (1/(dz*rho*A)*(mdot)*(T3-T2));
97      (1/(dz*rho*A)*(mdot)*(T_ret-T3))];
98
99  %Defining and evaluating the Jacobian Matrix with respect to T for
       discharging
100 JAC_CONV_T_DISCHARGING=jacobian(CONV_DISCHARGING(T1,T2,T3,mdot),[T1
       ,T2,T3]);
101
102 JAC_CONV_T_EVAL_DISCHARGING=matlabFunction(JAC_CONV_T_DISCHARGING);
103
104 %Defining and evaluating the Jacobian Matrix with respect to Mdot
       for discharging
105 JAC_CONV_mdot_DISCHARGING=jacobian(CONV_DISCHARGING(T1,T2,T3,mdot),
       mdot);
106
107 JAC_CONV_mdot_EVAL_DISCHARGING=matlabFunction(
       JAC_CONV_mdot_DISCHARGING);
108
109 %%% Defining the values for the Jacobian for the discharging, so it
        can be implemented in the
110 %%% observer
111 conv_dis_nom=CONV_DISCHARGING(T1nom,T2nom,T3nom,mdotnom);
112
113 jac_conv_dis_T=JAC_CONV_T_EVAL_DISCHARGING(mdotnom);
114
115 jac_conv_dis_mdot=JAC_CONV_mdot_EVAL_DISCHARGING(T1nom,T2nom,T3nom)
       ;
```

The Simulink setup:

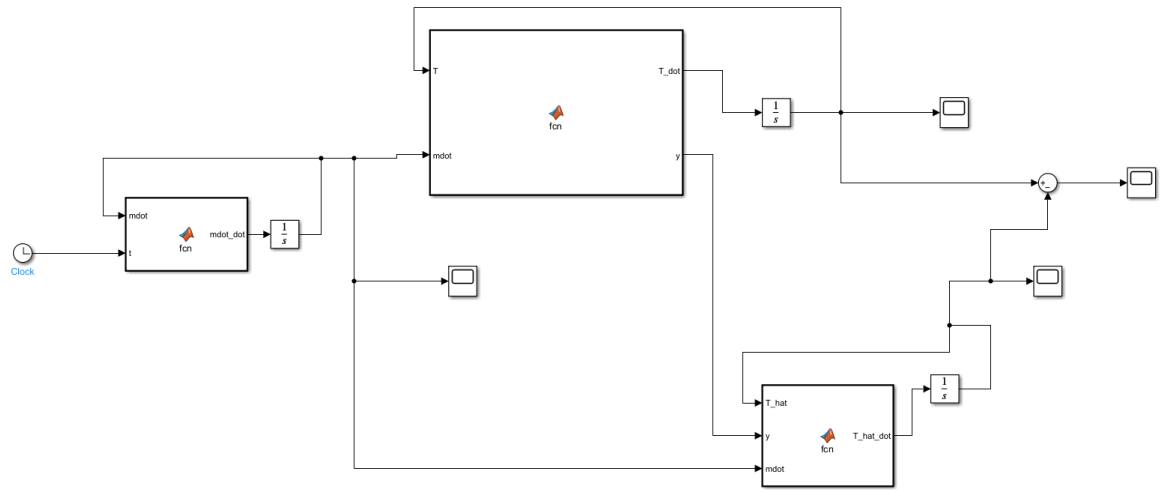

Figure 10: *Simulink setup*

The data from the left block of figure 10

```
function mdot_dot = fcn(mdot,t,K_mdot)
%%%This functions describes the charging and discharging of the
    system
%%%using an integrator to simulate a more real-life applications


%%%Refers to the different charging and discharging modes that mdot
     might
%%%have, 1=nothing, 2=charging, 3=discharging
mdot_ref1=0;

mdot_ref2=1;

mdot_ref3=-1;

%%% States between which seconds, charging, discharging or nothing
    happens
mdot_star=(0<=t)*(t<20)*(mdot_ref1)+(t>=20)*(t<=30)*mdot_ref2+(t
    >30)*(t<=40)*mdot_ref1+(t>40)*(t<=50)*mdot_ref3;


%%% The integrator
mdot_dot = -K_mdot*(mdot-mdot_star);
```

The data from the higher middle block of figure 10

```
function [T_dot,y] = fcn(T,mdot,rho, A, dz, T_amb, cp, P, k,T_ret,
    T_sup,alpha)
%%% This function describes the temperature of the "plant"

%%% Temperature dynamics of the layer
T1=T(1);
T2=T(2);
T3=T(3);

%%% Layer 1
conv1=(1/(dz*rho*A))*((mdot>=0)*abs(mdot)*(T_sup-T1)+(mdot<0)*abs(
    mdot)*(T2-T1));
lam1=(1/20)*log(1+exp(10*(T2-T1)));
T_dot1=(alpha/dz)*(T2-T1)+((P*k)/(rho*cp*A))*(T_amb-T1)+conv1+lam1;

%%% Layer 2
conv2=(1/(dz*rho*A))*((mdot>=0)*abs(mdot)*(T1-T2)+(mdot<0)*abs(mdot
    )*(T3-T2));
lam2=-(1/20)*log(1+exp(10*(T2-T1)))+(1/20)*log(1+exp(10*(T3-T2)));
T_dot2=(alpha/dz)*(T1+T3-2*T2)+((P*k)/(rho*cp*A))*(T_amb-T2)+conv2+
    lam2;


%%% Layer 3
```

```
conv3=(1/(dz*rho*A))*((mdot>=0)*abs(mdot)*(T2-T3)+(mdot<0)*abs(mdot
    )*(T_ret-T3));
lam3=-(1/20)*log(1+exp(10*(T3-T2)));
T_dot3=(alpha/dz)*(T2-T3)+((P*k)/(rho*cp*A))*(T_amb-T3)+conv3+lam3;



T_dot = [T_dot1;T_dot2;T_dot3];

%%% Temperature for reference for the observer
y=[T1;T3];
```

The data from the lower right block of figure 10

```
function T_hat_dot = fcn(T_hat,y,mdot,dz, rho, A, alpha, P, k,
    T_amb, Beta,cp,jac_lambda_nom, lambda_nom, T3nom, T2nom, T1nom,
    mdotnom, jac_conv_mdot, jac_conv_T, conv_nom,conv_dis_nom,
    jac_conv_dis_T, jac_conv_dis_mdot)

%%%Defining the temperature estimates
T_hat1 = T_hat(1);
T_hat2 = T_hat(2);
T_hat3 = T_hat(3);

%%%Defining the error in alpha as described in the report
alpha = 1.365*alpha;

%%% Defining y_hat so it can be fed into the temperature estimates
    as e_y
y_hat=[T_hat1;T_hat3];

e_y = y_hat-y;


%%% Feedback for the observer
T_c=[0,1,0;1,0,0;0,0,1];

Gn=[1,1;-1,0;0,-1];

v=Beta*[sign(e_y(1));sign(e_y(2))];

%%% Description of the temperature of each layer

%%% Layer 1
f1=(alpha/dz)*(T_hat2-T_hat1)+((P*k)/(rho*cp*A))*(T_amb-T_hat1);

%%% Layer 2
f2=(alpha/dz)*(T_hat1+T_hat3-2*T_hat2)+((P*k)/(rho*cp*A))*(T_amb-
    T_hat2);


%%%Layer 3
```

```
34 f3=(alpha/dz)*(T_hat2-T_hat3)+((P*k)/(rho*cp*A))*(T_amb-T_hat3);
35
36 %%%Describing the jacobian matrices for lambda, the convection when
37 %%%charging and the convection when discharging.
38 lambda_linearized=lambda_nom+jac_lambda_nom*(T_hat-[T1nom;T2nom;
      T3nom]);
39
40 conv_linearized=conv_nom+jac_conv_T*(T_hat-[T1nom;T2nom;T3nom])+
      jac_conv_mdot*(mdot-mdotnom);
41
42 conv_disc_linearized=conv_dis_nom+jac_conv_dis_T*(T_hat-[T1nom;
      T2nom;T3nom])+jac_conv_dis_mdot*(mdot-mdotnom);
43
44 %%% Describes the final temperature estimates. The discontinuous
      signal is
45 %%% inversed so it transfers back to the normal coordinate system.
46 %%% Furthermore it adds the errr in lambda and adds the linearized
      values
47 %%% for lambda, charging and discharging
48 T_hat_dot = [f1;f2;f3]+(eye(3)/T_c)*Gn*v+1.25*lambda_linearized+(
      mdot>0)*conv_linearized+(mdot<0)*conv_disc_linearized;
```